RSC Advances

Polymer nanocomposites foam filled with carbon nonmaterial's as an efficient electromagnetic interference shielding material

Journal:	*RSC Advances*
Manuscript ID:	RA-REV-02-2015-003409.R1
Article Type:	Review Article
Date Submitted by the Author:	15-Apr-2015
Complete List of Authors:	Dhakate, Sanjay; CSIR-National Physical Laboratory, New Delhi, Physics & Engineering of Carbon Subhedar, K.; CSIR-NPL, Materials Physics and Engineering Singh, Bhanu P.; CSIR, Physics and Engineering of Carbon

Polymer nanocomposites foam filled with carbon nonmaterials as an efficient electromagnetic interference shielding material

Sanjay R. Dhakate*, Kiran M. Subhedar and Bhanu Pratap Singh

Physics and Engineering of Carbon, Division of Materials Physics and Engineering,
Academy of Scientific and Innovative Research (AcSIR)
CSIR- National Physical Laboratory, New Delhi-12, India.

Among the different carbon nanomaterials filled polymer composites foam, graphene based foam gives the superior specific shielding effectiveness as compared to typical metals.

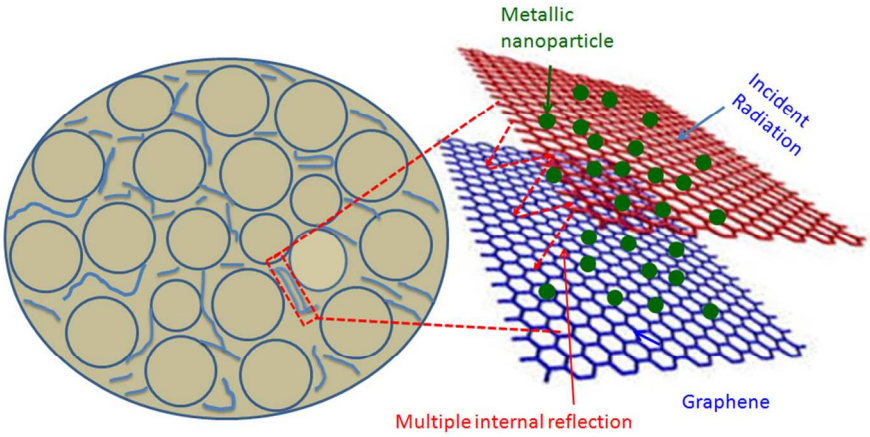

Polymer nanocomposites foam filled with carbon nonmaterials as an efficient electromagnetic interference shielding material

Sanjay R. Dhakate*, Kiran M. Subhedar and Bhanu Pratap Singh

Physics and Engineering of Carbon, Division of Materials Physics and Engineering,
Academy of Scientific and Innovative Research (AcSIR)
CSIR-National Physical Laboratory, New Delhi-12, India.

Abstract

With increasing use of newer and newer electronic gadgets in the modern society causes rapid growth of electromagnetic pollution which leads to detrimental effect on functioning of highly sensitive precision electronic equipments as well as on human life. Mitigate this effect requires efficient electromagnetic radiation shielding material which should be light weight, corrosion resistance and cost effective. In this review article we have presented light weight polymer composites foam filled with carbon nanofiber, carbon nanotubes and graphene as an efficient electromagnetic radiation shielding materials. It is seen that low loading of multiwalled carbon nanotubes with uniform dispersion in polymer, uniform cell size of pore with control dielectric constant resulted in to attenuation of electromagnetic radiation by adsorption phenomena. While chemical vapor deposition technique derived flexible graphene-polymer composite foam demonstrated the specific shielding effectiveness ~500 (333) $dB.cm^3/g$ is highest value among reported in literature. It is dominated mostly by absorption of electromagnetic radiation which is due to the multiple reflection of radiation inside the cells. Also different carbon nonmaterials such as carbon nanofiber and few layer graphene filled polymer composites foam with the varying content of conducting filler are reported in this review and which will be used in different applications, their future prospective and challenges ahead are discussed in this review.

* Corresponding author : dhakate@mail.nplindia.org (Sanjay R.Dhakate), Tel: 091-1145609388

1. Introduction

Contemporary electronics which are highly packed with integrated circuits creates severe electromagnetic radiation, which leads to harmful effects on functioning of highly sensitive precision electronic equipments as well as for human beings. High demands of today's technologically advanced fast moving society rely on the modern electronic gadgets (cellular phone, high-speed communication frameworks, military gadgets and wireless devices) which cause fast augmentation of electromagnetic radiation sources. To minimize the effect of these, electromagnetic interference (EMI) shielding of both electronics and the radiation sources are needed. EMI shielding refers to the blocking of electromagnetic (EM) radiation essentially cannot pass through blocking or shield material [1]. The main mechanism of EMI shielding is reflection and absorption of electromagnetic radiation. For reflection of the radiation, shield material must have mobile charge carriers, which interact with the electromagnetic field in the radiation. As a result, the shield material tends to be electrically conducting. The electrical conductivity is not scientific criteria for shielding, as conduction requires connectivity in the conduction path. Metals are the most widely used shielding materials but they suffer from problems such as high density, corrosion, difficult/ uneconomic processing and a low specific shielding capability [2]. So metal coating made by electroplating or vacuum deposition is commonly used for shielding [3-5]. Conductive layer can be put on substrate by different methods like silk-screen printing [6], vacuum evaporation or magnetron sputtering [7]. They found for deposition on different kind of surfaces an effective shielding coefficient was about 50 dB. But every material is not suitable for conductive coating [8]. While, polymers offer lightness, low cost, easy shaping, etc. The polymeric materials have been widely used in almost every sector of industry due to its unique properties and have been made lot of impact in the modern society. Nevertheless, most of them cannot prevent electromagnetic waves from propagating because of their electrical insulating properties. The best strategy to overcome this problem consists of dispersing electrically conductive fillers within polymer matrices [9]. These electrically conductive polymer composites are established much attention for EMI shielding applications, [10–23] because of their light weight, resistance to corrosion, flexibility, good processability, and low cost compared to the conventional metal-based materials. These conductive composites have different applications. Figure 1 shows the application of conductive composites as EMI shield with their conductivity values [24,25]. The EMI shielding

effectiveness (SE) of the polymer composites depends critically on the intrinsic electrical conductivity, dielectric constant, magnetic permeability, aspect ratio, and conten t of conductive fillers. It is believed that high electrical conductivity and connectivity of the conductive fillers can improve EMI shielding performance [10]. A major disadvantage of nanocomposites that contain conducting carbon nonomaterial or other fillers (nickeled carbon fibers, stainless steel fibers) [26], have a high tendency to reflect the electromagnetic radiation rather than to absorb it. Although these reflection can stops the wave propagation beyond the composite material, EMI overcome in the inner volume and as a result of multiple reflections from the walls. These reflections are root of damage, e.g., in the case of electronic circuits, because of unauthentic interferences between the constitutive electronic components (transistors, resistors and chips). For these deadly effects to be cancelled while preserving the shielding effect, the electromagnetic waves must be absorbed by the shield material and attenuated by conductive dissipation.

For an EMI shield material to absorb electromagnetic radiation, the dielectric constant must be as close to that of air as possible. The reflection of the signals results indeed from a mismatch between the wave impedances for the signal propagating into air and into the absorbing material, respectively, and the wave impedance is proportional to the inverse of the dielectric constant of the medium. A straightforward approach to this highly desirable situation may be found in the foaming of carbon nanomaterials containing polymers. The relative volume of air in open-cell foam is indeed very high, which is very encouraging for the matching of the wave impedances of the expanded material in the ambient atmosphere. The porous structure of these foams also provides additional benefit for EMI shielding due to the enhanced energy absorption by the wave scattering in the wall of pores. Carbon nanofibers, nanotubes and graphene, as compared to conventional metals and carbon fillers, have remarkable structural, mechanical, and electrical properties. The use of these carbon nanostructures as fillers in polymeric composites foam allows systems with low filler loadings to provide the desired electrical and EMI shielding properties [28-32] because of very high aspect ratio of these carbon nanofillers. This review article systematically reported the recent advances in the conducting polymeric foam filled with carbon nanofiber, nanotubes and graphene, their properties and applications. Finally, the challenges and the promising future of conducting light weight foam materials are discussed.

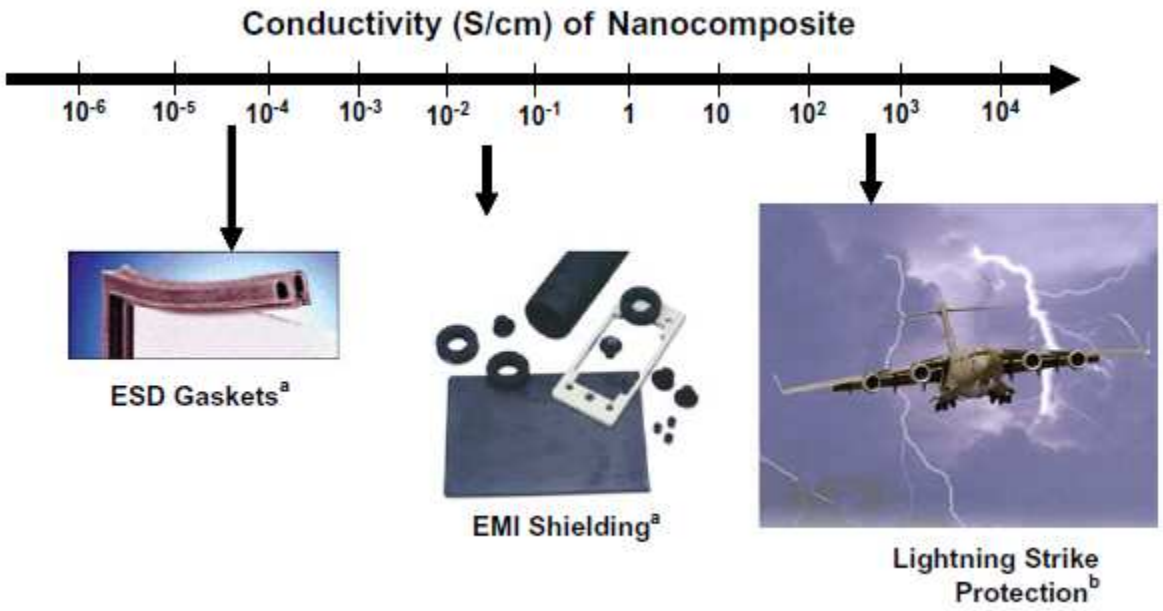

Figure 1: Different conductive nanomaterials -polymer composites potential application as shielding Material (Reproduced from Ref. 24,25).

2. Electromagnetic Shielding Effectiveness (SE)

The SE of a shield material is the ability to attenuate EM radiation that can be expressed in terms of ratio of incoming (incident) and outgoing (transmitted) power [33]. Higher values of SE in decibels (dB) signify less energy passes through the shield and most of the energy absorbed or reflected by shield material. It is well known that EMI-SE is sum of the reflection from material surface (SE_R), the absorption of electromagnetic energy (SE_A), and the multiple internal reflections (SE_M) of electromagnetic radiation. The reflection is related to the impedance mismatch between air and absorber, the absorption can be regarded as the energy dissipation of the electromagnetic microwave in the absorber and the multiple reflections are considered as the scattering effect of the in-homogeneity within the materials.

EM attenuation offered by shield depends on the above mentioned three mechanisms: reflection of the wave from the front face of shield, absorption of the wave as it passes through the shield and multiple reflections of the waves at various interfaces [34]. Therefore, total SE (SE_T) is attributed to three types of losses viz. reflection loss (SE_R), absorption loss (SE_A) and multiple reflection losses (SE_M) and it can be expressed as,

$$SE_T\,(dB) = SE_R + SE_A + SE_M = 10\log\,(P_t/P_i) \qquad \text{(i)}$$

Where, P_i and P_t are power of incident and transmitted EM waves respectively. It is significant to note that the losses associated with multiple reflections can be ignored (SE_M~0) when SE of EMI shielding material is more than -10 dB [35], so that SE can be expressed as

$$SE_T\,(dB) = SE_R + SE_A \qquad \text{(ii)}$$

In this review article the SE related to the reflection and absorption electromagnetic radiation from carbon nanomaterials filled polymers composites foam is discussed.

3. Carbon nanotubes –polymer composite foam

The carbon nanofiber reinforced polymer composites foam first time reported by Yang et al [36] as a conductive foam for EMI shielding material. The polystyrene (PS) composite foam reinforced with the different content of carbon nanofibers ranging from 0 to 20 wt % with foaming agent. The PS is insulating polymer possess very low value of conductivity and after incorporation of nanofibers conductivity increases significantly and it is continuously increases with increasing the nanofibers content in the composite foam. The percolation threshold of carbon nanofibers in composites foam is 5 wt%. Figure 2 shows the SEM micrograph of composite foam structure and the nature of the dispersed carbon nanofibers within the PS matrix. It is evident that foam structure is formed throughout the carbon nanofiber-polymer composites. At a relatively higher magnification (insert in Figure 2a) carbon nanofibers are dispersed and embedded throughout the PS matrix and interconnected carbon nanofiber structure is formed. The insulating behavior of pure PS does not exhibit any EMI SE while nanofiber-PS composite foam with increasing carbon nanofiber EMI SE increases significantly and it is independent of frequency in the X band frequency region.

The EMI SE of 1 wt % nanofiber-PS foam in less than 1 dB, on increasing nanofibers content 5, 10 and 15 wt % SE increases to 5, 14 and 19 dB. This demonstrates the main contribution for EMI SE comes from the nanofiber; it forms the conducting interconnected nanofiber network in the insulating PS matrix. On the other hand, it is well reported that carbon nanotubes exhibit remarkable structural and electrical properties compared to carbon nanofibers, such as smaller diameter, larger aspect ratio, higher electrical conductivity and strength. It seems logical to expect that with all these unique properties of carbon nanotubes, carbon nanotubes filled PS composite foam provide improved EMI SE.

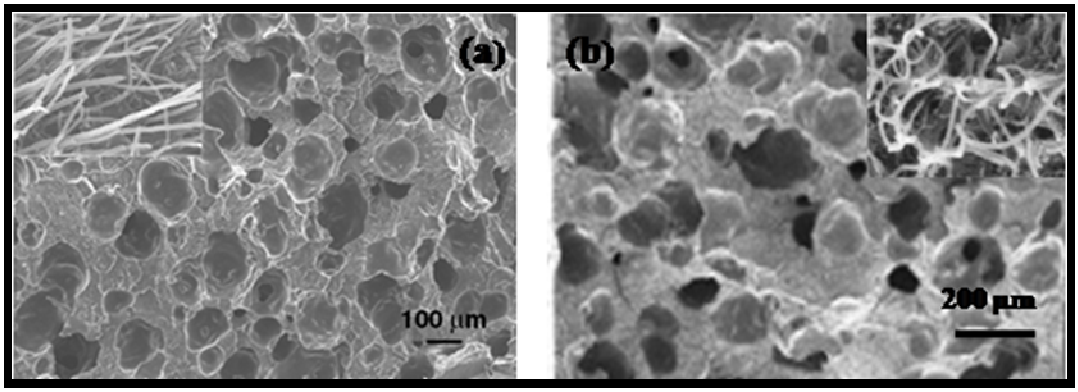

Figure 2: PS composite foam (a) filled with nanofiber, (b) filled with nanotubes. (Reproduced with permission from ref. 36 and 37. Copyright 2005 Wiley-VCH and 2005 American Chemical Society)

Society of Chemistry and 2014 American Chemical Society.In this direction, Yang et al [37] reported the carbon nanotubes-PS composites foam with varying carbon nanotubes content from 0 to 7 wt % and 5 wt % foaming agent. The SEM images (Figure 2b) of the cross section of the 5 wt % carbon nanotube-PS foam composite. The gas bubbles formed are almost spherical and uniform and the cell sizes range from 40 to 170 μm. The insert in Figure 2b shows the SEM image at higher magnification, it clearly demonstrate that carbon nanotubes are dispersed and embedded throughout the PS matrix and interconnected carbon nanotubes network is formed. This conductive nanotubes network established electrical conduction pathways throughout composite foam which is responsible for electrical conductivity. The CNTs-PS foam electrical conductivity increases with increasing CNTs content, the extent of increase is higher at higher content of CNTs as a consequence of conductive network formation in the insulating PS matrix. As depicted in Table 1, there is a noteworthy difference in the efficiency of carbon nanofiber and CNTs in imparting SE to the foam composites. The CNT-PS foam composite exhibited a higher SE (above 10 dB) compared to 3 dB for the CNF-PS foam composite at the same filler loading (3 wt %). Even the foam composite with 7 wt % CNTs gave an EMI SE comparable to that of the foam composite with 15 wt % carbon nanofibers. The difference in the results is originating from the fact that carbon nanotubes possess much smaller diameters and larger aspect ratios with higher electrical conductivities as compared to carbon nanofibers. The smaller size of the CNTs provides a larger interfacial area; therefore, the number of conductive interconnected nanotubes increases. And the larger aspect ratio of CNTs helps to create extensively continuous networks that facilitate electron transport in the foam composite with low nanotubes loading. As discussed

above, it reveals that the CNTs-PS composite foams are more effective in providing EMI shielding compared to the carbon nanofiber-PS composite foams.

Table 1: Average EMI SE of CNF-PS and CNT-PS Foam in X-band frequency range [reproduced with the permission from ref. 36, 37].

Fillar content (wt%)	CNF-PS	CNTs-PS
0.5	0.4	2.84
1	1.00	5.73
3	3.09	10.30
7	8.53	18.56
15	19.00	-

Xu et al [38] reported lightest conducting polymer composite foam (density of 0.05 g/cm ^{3}) based on multiwall carbon nanotubes and rigid polyurethane. The composite foams are prepared by static casting with blown agent (H_2O) and effect of blown agent on the density of foam and its relation with electrical conductivity of foam with 2wt % of MWCNTs loading is presented.

Figure 3a shows the typical morphology of the 0.05 g/cm^3 foam with a CNT loading of 2 wt.%. The cell wall of this ultralight conductive foam is much thinner. The shape of the cells is polyhedral rather than spherical owing to the squeezing among the cells that result from the high expansion ratio of the foaming. Figure 3b shows the conductivity–density relationship for the foam. The conductivity of about 2.4 x 10^{-2} S/m is registered with the density 0.51 g/cm^3. With a decrease in density from 0.51 to 0.05 g/cm^3, the conductivity declines gradually from approximately 2.4x 10^{-2} S/m to approximately 4.3x10^{-5} S/m. As the density is further reduced and approaches 0.03 g/cm^3, the conductivity exhibits a nonlinear abrupt decrease of about eight orders of magnitude, which indicates a conductor–insulator transition. With decreasing the density of foam, cell wall thickness decreases and during fast foaming process CNTs can hardly flow together with liquid resin in short duration. This results in the absence of nanotubes in the cell wall as a consequence nanotubes are more dense in the struts of low density foam while in higher density foam nanotubes are equally distributed in cell and struts.

At higher density, the cells assume regular spheres and the CNTs are uniformly distributed in the matrix. Both the cell walls and the struts construct the conductive pathways, thereby resulting in high conductivity. With the decrease in density, the cell walls get thinner and the cells become polyhedrons. The distribution of the CNTs becomes non uniform and the

nanotubes accumulate in the cell struts as the density decreases due to the growth of air bubbles. The conductivity decreases gradually with the density, as a result of the transition from 3D to 2D percolation and the decrease in CNT content in the cell walls, as well as the more porous structure of the composite.

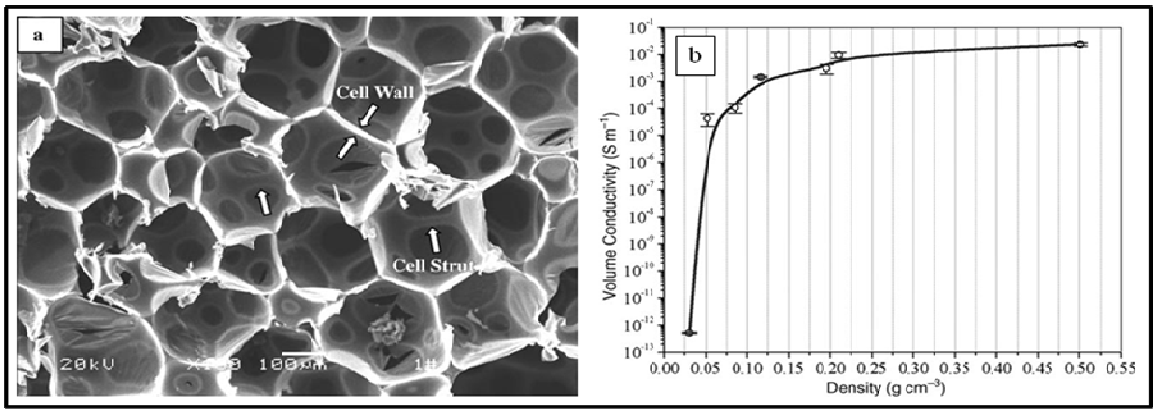

Figure 3: (a) SEM image of CNTs/ polyurethane foam of density 0.05 g/cm^3 and (b) variation in conductivity with density (Reproduced with permission from ref. 38. Copyright 2007 Wiley-VCH)

Thomassin et al [39], reported the MWCNTs/polycaprolactone (PCL) composites foam by supercritical CO_2 as foaming agent with the prospect of decreasing the material permittivity and thus reflectivity in order to prepare materials with high value EMI shielding. The carbon nanotubes are dispersed within PCL by melt-blending and by co-precipitation. The PCL foam are prepared by melt blending containing 0, 0.1 and 0.222 vol.% of MWCNTs and foam containing 0, 0.107 and 0.249 vol. % MWCNTs prepared by co-precipitation. Figure 4 compares the SEM micrographs for PCL foams containing 0, 0.222 and 0.249 vol % MWCNTs prepared by melt blending and by co-precipitation technique. The unloaded PCL foams exhibit a non uniform open-cell structure with pores larger than 100 mm (Figure 4a). Upon addition of 0.222 vol% MWCNTs, the porous morphology is better defined with smaller pores and a higher cell density (Figure 4b). The MWCNTs are playing two roles, it increases the internal viscosity at 60ºC and acting as nucleating agents, this leading to a larger number of cells growing to a smaller size. While in figure 4c, foam with 0.249 vol % MWCNTs prepared by co-precipitation method shows non uniform pore size.

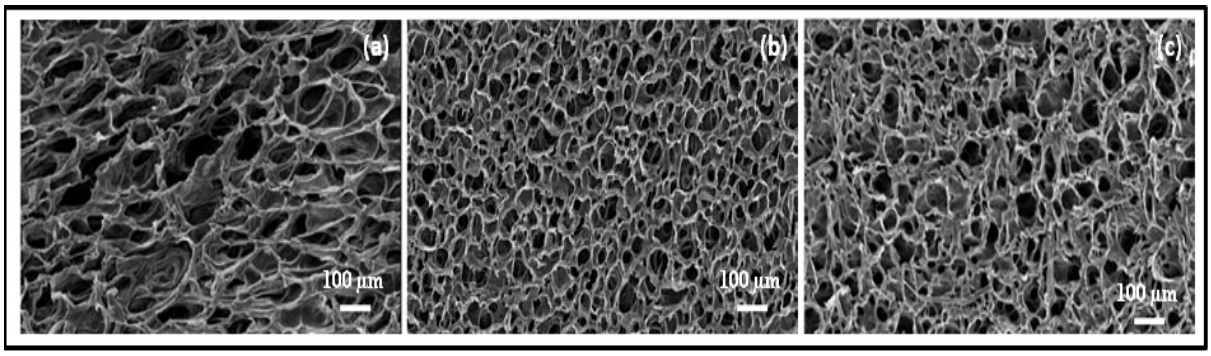

Figure 4: SEM micrographs of PCL foams filled with (a) 0 vol% of MWCNTs (b) 0.222 vol % MWCNTs (melt-blending) and (c) 0.249 vol % MWCNTs (co-precipitation). (Reproduced with permission from ref. 39. Copyright 2008 Royal Society of Chemistry)

Electrical conductivity is of the extreme importance for EMI performance, because it expresses the intrinsic ability of the material to absorb electromagnetic waves [40]. As a rule, a good electromagnetic absorber must exhibit a conductivity higher than 1 S/m and a real part of the effective dielectric constant as close to 1 as possible. The SE of the PCL foam containing 0.249 vol% of MWCNTs is in the 60 to 80 dB range, thus three to four times higher than the SE of the unfoamed counterpart. Herein, SE is directly proportional to the conductivity, which means that SE is increased by a factor of two whenever the conductivity is doubled. The direct proportionality between SE and conductivity is reported in Figure 5a and b, which indicates that the shielding effect actually results from the absorption of the incident signal power entering the composite foam and its conductive dissipation through the material thickness. This is revealed by the experimental reflectivity (R), which is quite an important characteristic feature of EMI shielding and microwave absorbing materials. It depends on the mismatch between the dielectric constants of the material and the surrounding atmosphere (air). In order to minimize the reflectivity, the dielectric constant of the material must be as close to unity as possible. It is however known that dispersion of a conductive additive within an insulating polymer results in a higher dielectric constant proportional to the final conductivity [41]. The foaming of nanocomposites allows the dielectric constant to be maintained below 4, even at the higher conductivity observed, as illustrated in Figure 5c by the comparison of the dielectric constants of the unfoamed and foamed samples. For the sake of comparison, the dielectric constants of

foamed and unfoamed PCL are also reported. The dielectric constant of the PCL foam is close to one (1.2), nearly two times lower than that of unexpanded PCL (2.2). For this reason, the dielectric constant of foamed PCL filled with 0.24 vol% MWCNT (3.5 at 30 GHz) is comparable to those of unfoamed PCL containing 0.16 and 0.48 vol% of nanotubes (between 3 and 4), although the conductivity is roughly 3 to 4 times higher. Moreover foamed PCL with 0.107 vol% MWCNT, which exhibits similar SE as the 0.16 vol% MWCNT filled unfoamed PCL (28 dB vs. 24.2 dB at 30 GHz), exhibits a much lower reflectivity (12.25 dB vs. 10.5 dB at 30 GHz), as result of a lower dielectric constant (2.35 vs. 3.3 at 30 GHz). Foaming of PCL nanocomposites is thus an easy and effective way to provide carbon nanotube filled polyesters with a highly desirable combination of shielding efficiency in the 20–80 dB range and reflectivity lying between 15 and 8 dB. These performances are superior [36,37] to reported in Table 1, for foams loaded with 15 wt% carbon fibers, for which the EMI shielding mainly originates from a high reflectivity. Indeed, the 15 wt% loading is responsible for a high dielectric constant (>30) and thus a reflection phenomenon at the input interface. Similarly, PS foams loaded with 7 wt% carbon nanotubes have a SE of 20 dB together with a reflectivity of only 1.83 dB (R = 0.81). Again, reflection is the major contribution to the EMI shielding rather than absorption. The foaming of the nanocomposites decreases the dielectric constant and thus the reflection at the input interface, whereas the proper dispersion of the CNTs within the polymer provides, even at a low loading (<1 vol%), a conductivity high enough for electromagnetic waves to be attenuated by conductive dissipation. The strategy reported in this work is thus basically different from that previously reported [36,37] because the EMI reduction is the result of absorption at low filler content, and not of reflection at relatively high filler content via a higher dielectric constant.

Herman [42], reported conductive styrene/divinylbenzene (DVB) based poly high-internal phase emulsions (HIPEs)–single-walled carbon nanotubes (SWCNT) composite foams by utilizing the self-assembly of SWCNTs on a water–oil interface. The use of amphiphilic blocks copolymer-stabilized SWCNTs as Pickering stabilizers for the preparation of poly HIPEs has been shown to work efficiently. The morphology of the resultant foams is highly dependent on the loading of SWCNTs. With increasing the SWCNTs content, there is marked change in the foam morphology is reported and average void size decreases from 500 μm to 50 μm. The decrease in average pore diameter, consequently increase in total pore area with increase in SWCNT

loading. This reveals that the connectivity of the voids in the foam is dependent on the loading of SWCNT. The conductive composite foams with 0.007 wt% SWCNTs loading gives a

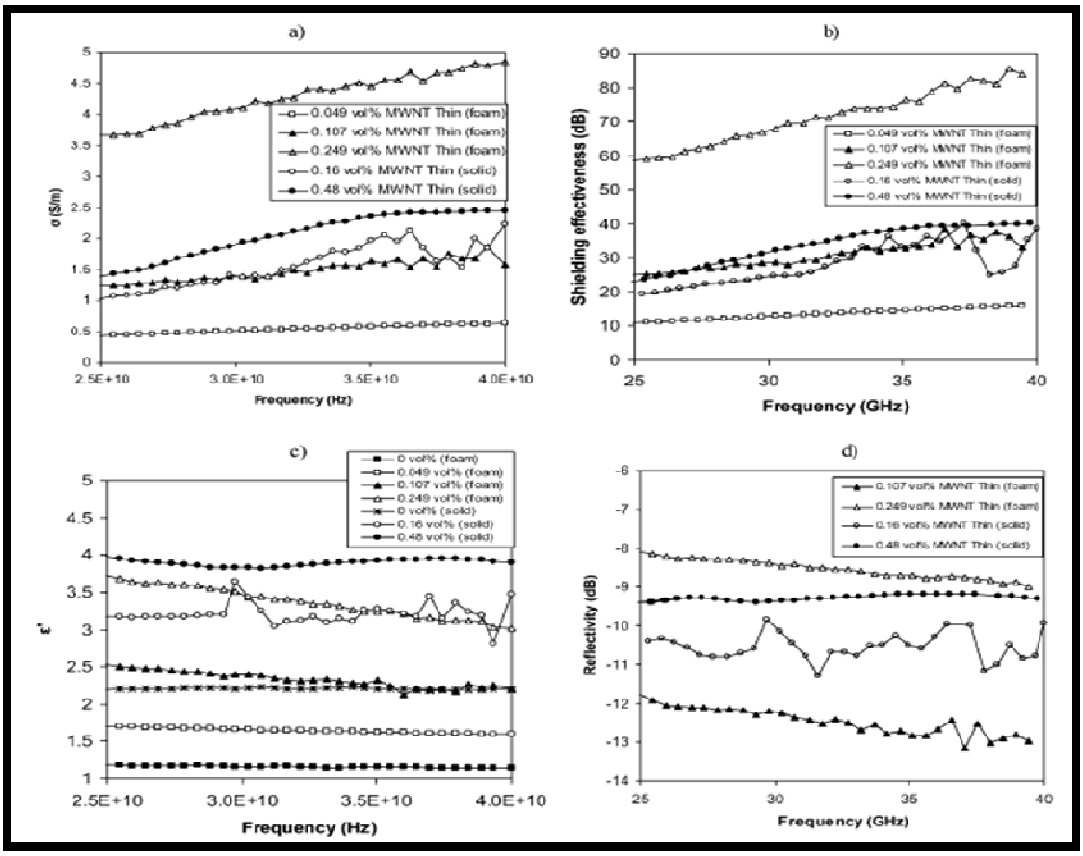

Figure 5: Electromagnetic properties of foamed and unfoamed MWNT/PCL nanocomposites prepared by co-precipitation: (a) conductivity, (b) shielding efficiency SE, (c) dielectric constant and (d) reflectivity R (Reproduced with permission from ref. 39. Copyright 2008 Royal Society of Chemistry)

conductivity of 10^{-3}S/m. This value of conductivity is sufficient for anti-static and EMI shielding applications. The conductivities of these foams appear to be independent of the loadings of conductive nanofiller SWCNTs.

Fletcher et al [43] have taken first time initiative to develop novel elastomer foamed nanocomposites. The fluorocarbon polymer is used extensively in aerospace industry because it offers robust physical properties, good high temperature properties (200ºC) and great sealing force retention. The fluorocarbon polymer -MWCNT composites up to 12 wt % of MWCNTs and fluorocarbon polymer -MWCNT composite foams are developed by using Celogen CE as

foaming agent. The conductivity of the elastomer nanocomposite at varying loading levels is shown in Figure 6a. The percolation threshold of about 2–3 wt% of MWCNTs and a saturated conductivity is at about 8wt% of MWCNTs. The foamed samples reached percolation a little behind the non-foamed, but reached saturation at about the same time. While the saturation conductivity for the foamed is the same as that of non-foamed. The density for the non-foamed and foamed is 1.7 g/cm^3 and 1.2 g/cm^3; there is 30% weight reduction. This demonstrate that lighter weight foamed material can be used with no conductivity penalty. The percolation threshold is at about 2% carbon nanotubes and the saturation of conductivity occurs at 8% carbon nanotubes by weight.

The SE of non-foamed and foamed elastomer nanocomposites for 3.8 mm thick sample increases as a function of loading level (Figure 6b & c) and as a function of thickness. While the conductivity saturates at approximately 6 wt %, the SE continues to increase with higher loading levels. Twelve percent loading gives a SE of 50 dB, while 6% loading gives 22 dB. However, there is not much difference between the SE of the foamed samples compared to the non-foamed. At 12% loading the difference is only 8%, at lower loadings it is less. This means that the weight can be reduced by 30% with only an 8% loss of SE. The permittivity and the electric loss factor for both non-foamed and foamed are reported [58]. Generally the permittivity increases with loading; however, the data is erratic for loadings between 6% and 10%. And although the scatter is greater with permittivity compared to SE; the permittivity of the foamed elastomer nanocomposites is equivalent to the non-foamed. The electric loss factor is not quite as unreliable and the values for foamed and non-foamed are comparable. This irregularity in the monotonic increase of permittivity as compared to SE indicates that there is a structural component of the material that is affecting the phase of the transmitted energy but not the magnitude. This could indicate the occurrence of a preferential alignment of nanotubes and the onset of saturation in the 6%, 8%, and 10% CNTs loadings. The combination of electrical properties with the flexibility and fluid resistance of fluorocarbon yields to a versatile light weight material.

Most of the existing polymer nanocomposite foams have low temperature thermoplastic matrices with a glass transition temperature (Tg) ranging between -65 and 105°C and a melting temperature ranging from 65 to 240°C, including polyvinylidene fluoride, poly(methyl methacrylate), polystyrene and low-density polymer ethylene [36-37,44-50]. For applications for

high service temperature required the high Tg and high melting temperature polymer nanocomposite foam.

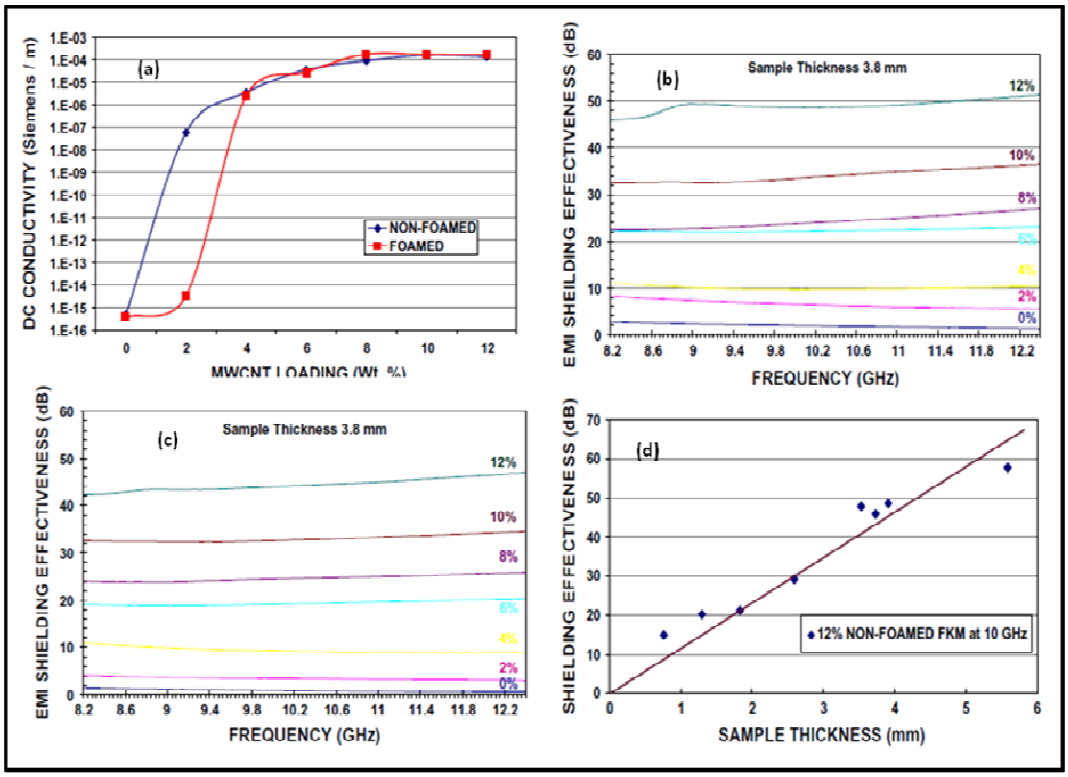

Figure 6:(a) Electrical conductivity of MWCNT loaded elastomer, (b) Shielding effectiveness of non-foamed elastomer nanocomposites, (c) Shielding effectiveness of foamed elastomer nanocomposites, (d) Shielding effectiveness as a function of sample thickness.
(Reproduced with permission from ref. 43. Copyright 2010 Elsevier)

The polyetherimide (PEI) a kind of high-performance polymer, possesses a high glass transition temperature (Tg) of 215°C, low smoke generation, desirable flame retardancy, and excellent mechanical properties. Kim et al [51] reported PEI/ MWCNTs nanocomposites with varying MWCNTs content from 0.5–3 wt% by solvent casting method. The PEI/MWCNT nanocomposites are foamed using a solid-state foaming method. Solid-state foaming is a two-stage process. The sample is first saturated in high-pressure CO_2 using a syringe pump and then foamed using hot platens [52]. The volume electrical conductivities of the PEI/MWCNT composites and their foams are dramatically increases between 0.5 and 1 wt% of MWCNT loading. The percolation threshold is determined by power law relationship [53]. The percolation threshold of PEI/MWCNT composites is found to be between 0.5 and 1 wt% for the

volume electrical conductivity. Foaming did not shift the percolation threshold but reduced the electrical conductivity. The electrical conductivity of the composite foams depended on the relative density. Foams with a higher relative density had a higher electrical conductivity. Despite the volume expansion due to foaming, the polyetherimide nanocomposite foams possess an electrical conductivity of 10^{-7} S/cm at 2 wt% carbon nanotube loading and 45% relative density. The fabricated PEI nanocomposite foams are thermally stable, with a Tg that is almost the same as that of the original PEI. The storage modulus of MWCNT-reinforced foams is higher than that of the neat PEI foams with a similar relative density. With the high performance polymer matrix, the nanocomposite foams fabricated low-density electrostatic dissipation applications in high temperature and high mechanical stress situations.

In recent decades, nanocomposite microcellular foams have attracted a great interest due to their high toughness, high stiffness, high thermal stability and low dielectric constant [54-56]. The microcellular foams when the cell density is greater than 10^9 cells per cm^3 of solid polymer and the average cell diameter is in the order of 10 nm [57]. Recently, Tran et al [58] demonstrated the microcellular foams of /MWCNTs/ poly (methyl methacrylate) PMMA with different content of MWCNTs by using supercritical carbon dioxide as a physical foaming agent. The effect of the foaming conditions (temperature and pressure) on the foams morphology (pore size, cell density, volume expansion cell-wall thickness) and its relation with conductivity is reported.

The pore size of neat PMMA and MWCNTs/PMMA foams is increases with increase in processing temperature (Figure 7a). But the MWCNTs/PMMA foam has smaller pore size than that of neat PMMA foam prepared under same condition. The cell density decreases with the foaming temperature for both neat PMMA and MWCNTs-PMMA foams. The decrease of the cell density with the increase of temperature follows the nucleation theory [59,60]. The expansion volume steadily increases with foaming temperature and it follows the same trend in both cases [58]. The volume expansion do not depends upon the amount of MWCNTs; it is directly proportional to pore size and number of nucleation sites. The MWCNTs in the polymer composite is acting as nucleating agent. The cell density and volume expansion increases when increases amount of CNTs. The cell density of the neat PMMA foam is smaller than the cell density of the PMMA -MWCNTs foam [61]. These observations are also in agreement with Lee et al. [52] and with the nucleation theory. When the same foaming conditions are used for both samples (neat PMMA and MWCNTs/PMMA), the nanofiller is acting as heterogeneous

nucleating agent in the nanocomposites, thus increasing the cell density compared to neat PMMA.

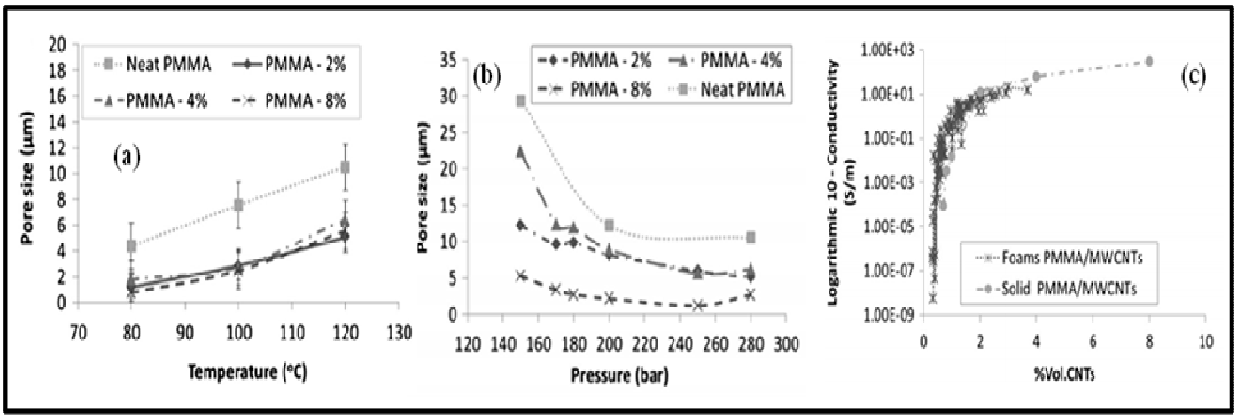

Figure 7: Variation in pore size in PMMA and PMMA-MWCNTs foam with (a) temperature (b) pressure and (c) conductivity with increasing MWCNTs content (Reproduced with permission from ref. 58. Copyright 2013 Elsevier)

The influence of the foaming temperature on cell-wall thickness demonstrated that cell-wall thickness for neat PMMA slightly decreases when increasing the temperature from 100 °C to120 °C. The cell-wall thickness of MWCNTs/PMMA is much lower due to the smaller pore size. A slight increase with the temperature is observed which is more pronounced when the CNTs content is very high (8 wt %) due to smaller increase in volume expansion [58].

The influence of pressure on foam morphology at temperature around the glass transition temperature (Tg) of PMMA (120°C). An increase of pressure from 150 to 280 bar induces a considerable decrease of the pore and cell size for both neat PMMA and MWCNTs/ PMMA, while uniform and homogenous cells are maintained over the whole pressure range. For neat PMMA, the pore size decreases from 29.4 to 12.2mm when increasing the pressure from 150 to 200 bar. Similarly, a significant decrease of the pore size is reported for PMMA loaded with 2 and 4 wt% of MWCNTs in the range of 150 bar (Figure 7 b).

The electrical conductivity of MWCNTs/PMMA solid composite increases with increasing the amount of MWCNTs in the PMMA matrix leads to the sharp enhancement of conductivity. In the case of foamed samples, the electrical conductivity strongly depends on the content of the conducting nano filler. Importantly, for the same MWCNT content, foamed nanocomposites present a much higher conductivity compared to solid ones. For instance, a conductivity of 1.7

S/m is measured for the foams containing 0.69 Vol% MWCNTs compared to less than 0.02 S/m for the solid sample with the same MWCNTs content. A lower percolation threshold is therefore reported for the foams (Figure 7c).

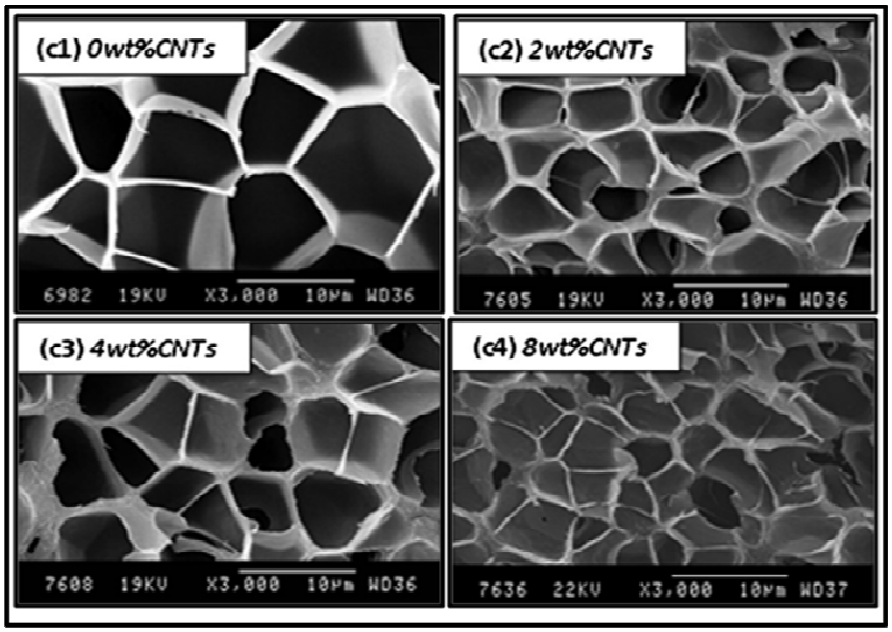

Figure 8: SEM images of foam with increasing MWCNTs content in PMMA.(Reproduced with permission from ref. 58. Copyright 2013 Elsevier)

Figure 8 shows SEM imgaes of MWCNTs/PMMA composite foam with increasing the MWCNTs content. It deomstrated that with increasing CNTs content the pore size decreases and cell density increases. The homogenous morphology of close cell maintained in all over the foams. The cell wall thickness also decreases with increasing the MWCNTs content [58].

Although CNTs have received much attention as they impart insulating polymers with high electrical and EMI shielding properties, their wider applications are still limited because of their disadvantages, such as high cost, impurities from the catalysts, bundling, and aggregation [63].

Ameli et al [65], reported the development of sets of nano/microcellular MWCNT/ polypropylene composites with varying the MWCNTs content, studied their electrical conductivity, dielectric permittivity and dielectric loss. Figure 9a shows the variation of the electrical conductivity of the nanocomposite foams with varying relative density containing different content of MWCNT. The electrical conductivity is found to increase with the decrease of the relative density up to an optimum relative density, which resulted in the maximum

conductivity value, up to two orders of magnitude higher than that of the corresponding solid sample. At the optimum relative density, the conductivity of 2.56 vol. % MWCNT/PP increases by 6.4 times while that of 0.51 vol.% MWCNT/ PP increases by more than 300 times, compared to those of the solid precursors.

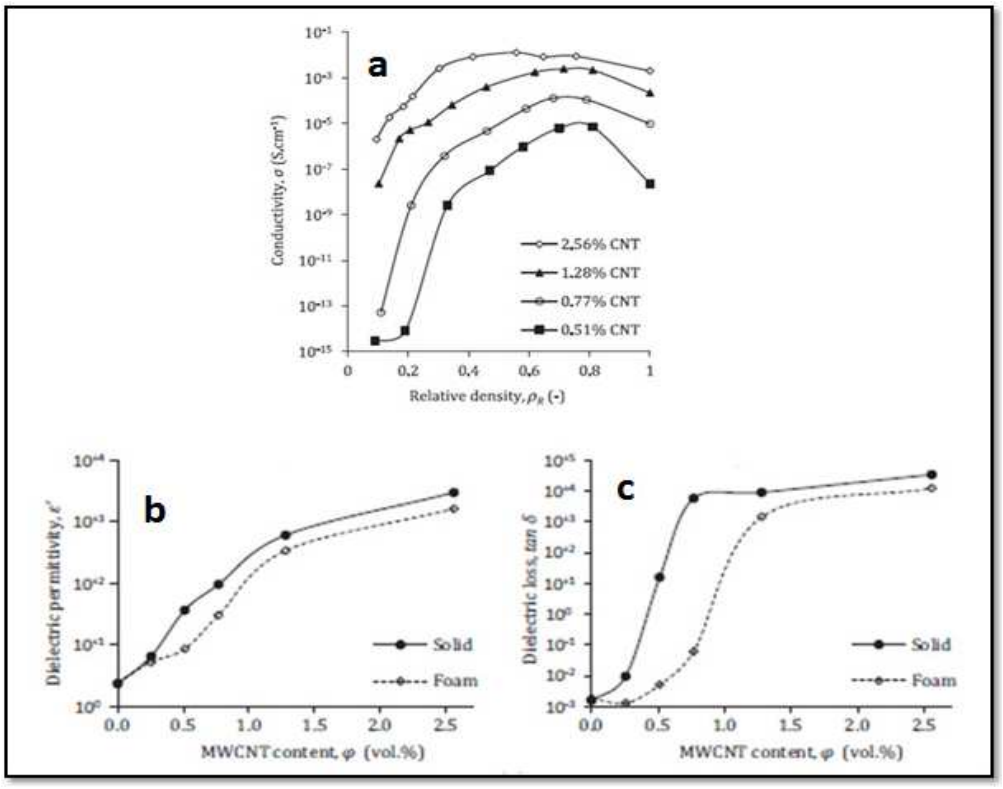

Figure 9(a) Electrical conductivity of nano/microcellular PP nanocomposites with different vol% MWCNTs as a functio of relative density , (b) dielectric permittivity (c) dielectric loss for foam MWCNT/PP nanocomposites measured at frequency fo 100 Hz (Reproduced with permission from ref. 65. Copyright 2014 Elsevier)

Figure 9b and c show the dielectric permittivity and loss of solid and foamed nanocomposites which is measured at 100 Hz frequency as a function of MWCNT content. In the solid nanocomposites, the dielectric permittivity continuously increases from 2.4 $X10^0$ to 3.0 X 10^3 with the increase of MWCNT contents. At 0.77 vol. % MWCNT, the dielectric permittivity of the solid samples is decreases from 96 to 30 when foaming was applied. However, the high dielectric permittivity (e' = 96) of the solid nanocomposites at 0.77 vol.%

MWCNT/PP is frequency dependent while that of the foamed counterpart revealed a frequency independent behavior.

The dielectic loss of the solid composite samples increases dramatically with the MWCNT content (figure 9c). Specifically, near the percolation threshold, when the MWCNT content is increases from 0.26 to 0.77 vol.%, the dielectric loss of the solid samples is enormously increases (up to 6 orders of magnitude). Unlike the high dielectric permittivity of the solid samples at high filler loadings, their very high dielectric loss limits their application as dielectric materials. The dielectric loss of the nanocomposite, however, significantly decreases when the foaming is introduced.

PP foams containing only 0.34 vol. % MWCNT presented a high dielectric permittivity (30) and very low dielectric loss (0.06). These significant improvements in dielectric properties are attributed to the decreases interconnections and interspace distances between MWCNTs caused by biaxial stretching and uniaxial compression effects of foaming action. They proposed the use of nano/microcellular MWCNT/polypropylene as an efficient EMI shielding as well as in charge storage.

By contrast, graphene sheets are believed to be an alternative of CNTs to prepare multifunctional polymer nanocomposites and foams, because of their high specific surface area, high aspect ratio, and layered structure [64].

4. Graphene –polymer composite foam

Graphene has been the subject of a wealth of scientific research and received much attention in all over world since early reports published by Geim and Novoselov in 2004. Graphene sheets, one atom thick two-dimensional layers of sp^2 bonded carbon atoms are predicted to have unusual properties. One possible route to harness these properties for applications would be to incorporate graphene sheets in a composite material [66]. Graphene based composites have many advantages for EMI shielding due to its low cost, high aspect ratio, and light weight. The low price and availability of the pristine graphite in large quantities coupled with relatively simple solution process makes graphene a potential choice as conductive filler in the preparation of conductive foam composites.

Eswaraiah et al [67] reported the novel graphene based polymer foam composites that can be used for broad EMI shielding applications. The few layer graphene having thickness 2-3 nm and lateral dimensions of 20 -40 m [68] are functionalized by acid treatment and used for the

fabrication of functionalized graphene (f-G) and polyvinylidene fluoride (PVDF) composites foam in which 2,2'-azobisisobutyronitile used as foaming agent. The different f-G-PVDF composite foams with varying f-G content from 0-11 wt% are presented. Figure 10a, shows the SEM image of the foam structure in which formation of micropores and cells are distributed all over the area, insert of figure 10a shows the ultrathin graphene sheets with the pores in the PVDF foam composites. The f-G nanofillers embedded in PVDF matrix with sufficient interconnections. The huge surface area and hence high aspect ratio of the f-G provides large number of interconnections with the estimated cell size in the range of 0.5 to 2.0 μm. This type of morphology of interconnection helps in achieving percolation in electrical conduction at lower loading, leading to the electrically conductive f-G-PVDF composite foams. It is demonstrated that below 0.5 wt % of f-G in PVDF, conductivity changes dramatically displaying an increase of thirteen order of magnitude and conductivity increases from 10^{-16} S/m to 10^{-3} S/m. The conductivity increases with f-G content and at 2 wt % it reaches to 10.16 S/m, thereafter there is no significant improvement in the conductivity value.

The EMI SE of f-G /PVDF foam composites in X-band region and broad band are displayed in figure 10 (b and c), it increases with increasing the f-G loading in PVDF foam composite. The SE of 1 and 5 wt % f-G in PVDF foam composite is 7 and 18 dB in the frequency range of 8–12 GHz. Similarly an EMI shielding efficiency of 20 and 28 dB has been obtained for 5 and 7 wt.-% f-G in broadband frequency range (1–8 GHz). The higher EMI shielding efficiency (28 dB) of the foam composites in broadband range (1–8 GHz) for 7 wt.-% f-G/PVDF in comparison to EMI shielding efficiency (20 dB) of 7 wt.-% f-G/PVDF composite in X-band is due to the skin effect of the foam composite at higher frequencies. The increase in EMI SE can be attributed to the increase in conductivity of the foam composite since graphene nanofillers formed a conducting network in PVDF matrix. As the loading of f-G increases in the polymer, the number of conducting f-G interconnections increases resulting in more interaction between the nanofillers and incoming radiation. This improves the shielding effectively. The EMI shielding mechanism in the present f-G/PVDF composites is reflection and which is confirmed by the observation of reflectivity of 5 wt.-% f-G/PVDF foam. The reflectivity (R), transmissivity (T), and absorptivity (A) are 0.78, 0.01, and 0.21, respectively for the foam containing 5wt.-% f-G and the result is consistent with the EMI shielding mechanism in pure graphene film[83]. As the mass fraction of f-G increases from 1 to 5 wt.-%, the reflectivity increases from10 to 80% of the

incident electromagnetic radiation. This reflection can be due to high electrical conductivity might be originated from change in the permittivity and dielectric losses of the f-G/PVDF foam composites.

In addition, tensile strength, ductility, and fracture toughness are also important properties for the application of polymer foams. It is well reported that the pores in polymer foam are very large; they would readily evolve to large cracks and make the foam brittle. Interestingly, microcellular foams can provide increased toughness, improved fatigue life and energy absorption [70,71]. In this direction, Zhang et al [44], reported tough polymethylmethacrylate graphene/PMMA nanocomposite microcellular foams are prepared by blending of PMMA with graphene sheets followed by foaming with subcritical CO_2 as an environmentally benign foaming agent.

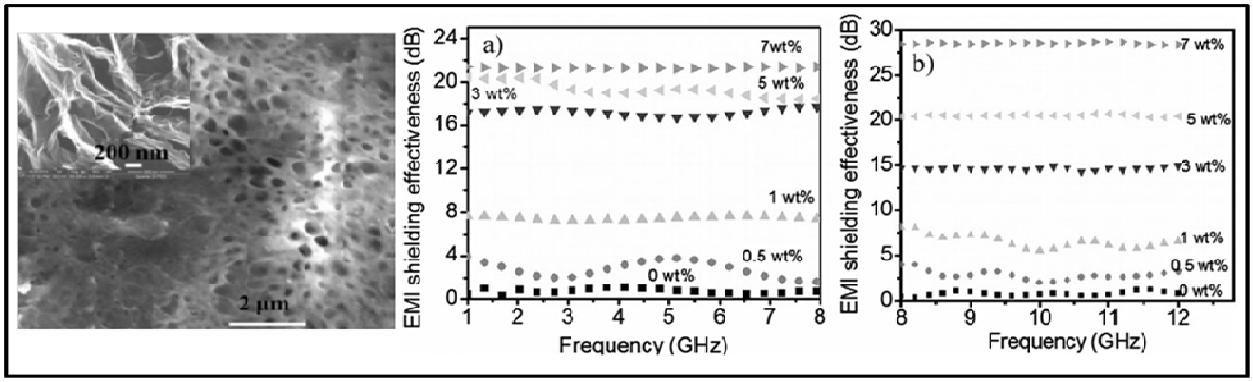

Figure 10: (a) SEM image of f-G/ PVDF composite foam (b) EMI SE with increasing MWCNTs content. Reproduced with permission from ref. 67. Copyright 2011 Wiley-VCH

The graphene/PMMA composite foams developed by solution blending and compounding method with varying the graphene content from 0 to 5 wt % of graphene (~3-4 individual sheets) [72]. Figure 11(a) shows SEM image of the cross section of the graphene/PMMA nanocomposite foam with 1.8 vol % graphene sheets. It is evident that the microcellular cells with an average size of 5 μm are distributed throughout the foam. These are nearly spherical cells exhibit a cell size distribution from 1 to 10 μm. This microcellular structure may offer advantages in improving electrical and mechanical properties of the foam over the polymer foams with larger cells that filled with carbon nanofibers and nanotubes. [36-38,45]. The formation of this unique microcellular structure is attributed to the use of subcritical CO_2 as the foaming agent. It is reported that, even a low (0.2 vol. %) loading of graphene sheets are

efficient in inducing the heterogeneous nucleation of cells and decreasing the cell sizes of the PMMA foam. The electrical conductivity increases with the increase of graphene content for both the bulk and foamed nanocomposites. Interestingly, the insulator-to-semiconductor transition of the foams shifts to lower graphene content compared to that of the bulk nanocomposites. The nanocomposite foam with 0.6 vol % graphene sheets has an electrical conductivity of 3.80 x 10^{-5} S/m, which satisfies the antistatic criterion of 1 x 10^{-6} S/m [73]. With 0.8 vol % of graphene sheets, the conductivity of the PMMA foam approaches to 0.39 S/m. A much higher conductivity of 3.11 S/m is obtained in the microcelluar foam with only 1.8 vol % of graphene sheets, which is higher than the target conductivity value required for EMI

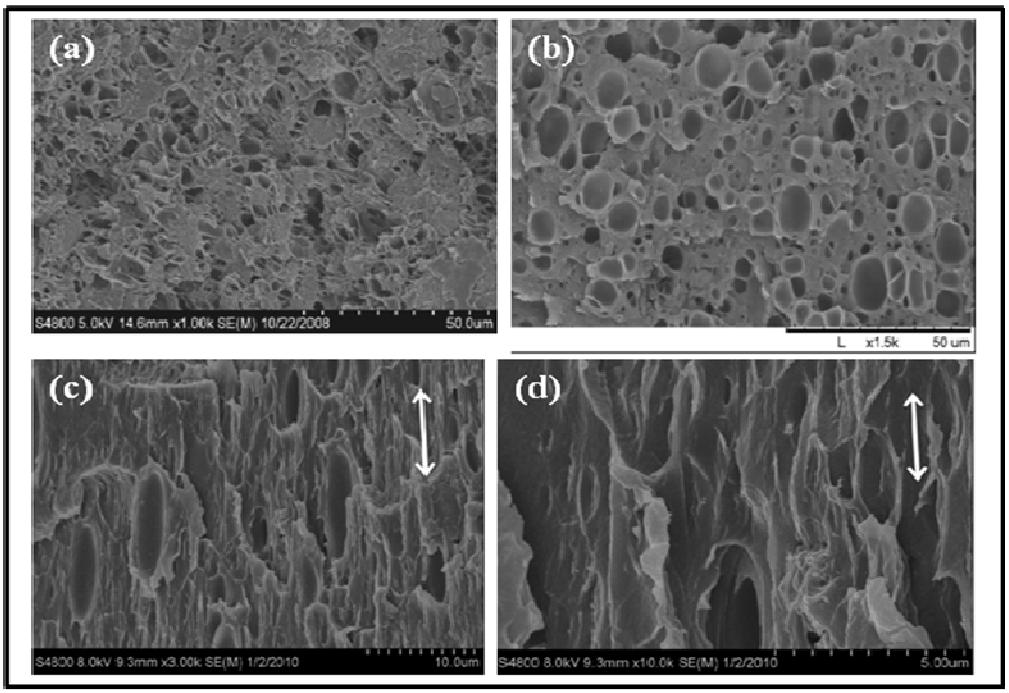

Figure 11: (a) SEM image of the cross-section of PMMA nanocomposite microcellular foam with 1.8 vol % graphene sheets, SEM images of 0.5 wt % graphene/ PMMA nanocomposite microcellular foam: (b) before stretching; (c) highly entangled microcellular cells near the fracture surface; (d) plastically stretched void network (Reproduced with permission from ref. 44, Copyright 2011 American Chemical Society)

shielding application [45]. The neat PMMA foam is transparent to electromagnetic waves and exhibits very small value of EMI (2.5 dB) shielding efficiency in the frequency range 8 -12 GHz. In contrast, with the increase of the graphene content, the EMI SE of the graphene/ PMMA

foams increases significantly which is similar to the relationship between electrical conductivity and nanofiller content and it is consistent with the EMI shielding theory [74]. SE total of the microcellular foam with 0.6 vol% graphene sheets is slightly higher than that of neat PMMA foam. However, when the graphene content is just increases to 0.8 vol %, the SE_{total} value is above 7.5 dB in the entire frequency range and approaches to 12 dB at the frequencies around 9.0 and 9.6 GHz. Furthermore, the microcellular foam with only 1.8 vol % graphene sheets exhibits high EMI SE of 13-19 dB at the frequencies from 8 to 12 GHz. This clearly demonstrates that EMI shielding properties of the graphene/PMMA foams results from the formation of an interconnected graphene network throughout the insulating PMMA matrix [75].

The SE_{Total}, SE_R, and SE_A of the graphene/PMMA nanocomposite foams as a function of graphene content at the frequency of 9 GHz. The increase of graphene content leads to the improvement of both SE_{total} and SE_A and the contribution of microwave reflection is negligible over all the graphene contents. For the nanocomposite foam with 1.8 vol % graphene sheets, the values of SE_{Total}, SE_A, and SE_R are 19, 18, and 1 dB, respectively. Therefore, the EMI shielding effect resulted from the absorption of the incident signal power entering the composite and its conductive dissipation through the nanocomposite foam thickness, confirming that microwave absorption is the dominant contribution to the SE_{Total} of the graphene/PMMA microcellular foams. As EMI SE generally increases with increasing the specimen thickness [76], but SE due to absorption is proportional to skin depth and for good absorbing material shielding should posses high conductivity, high permeability and sufficient thickness to achieve skin depth [77]. It is reasonable to expect that the EMI SE value for the PMMA foam can be improved by increasing the specimen thickness and the graphene content. Even with the low loading of graphene sheets (1.8vol%) and thin specimen (2.4 mm), the graphene/PMMA nanocomposite foam still exhibits a good EMI shielding (19 dB) effect, which is close to the target value of EMI SE required for practical application (20 dB). This indicates that graphene/PMMA nanocomposite microcellular foam is used as an effective and lightweight EMI shielding material. Besides reflection and absorption, multiple reflections are another shielding mechanism, which refers to the reflection at various surfaces or interfaces in the shield [78]. This mechanism requires the presence of a large surface area or interface area in the shield. The microcellular structures of graphene/PMMA foams provided a large cell-PMMA surface area, meanwhile the large specific surface area of graphene and its uniform dispersion in the matrix

formed abundant graphene/PMMA interfacial area. Therefore, it is reasonable that the unique construction formed by graphene sheets in the graphene/PMMA foam favors microwave absorption. Incident microwaves entering the graphene/PMMA microcellular foam are reflected and scattered many times between cell-matrix interfaces and the graphene sheets, and are difficult to escape from the material until they absorbed, similar to the case in ordered mesoporous carbon/ fused silica composites [79]. Thus, the contribution of absorption to the total EMI SE of the graphene/PMMA foam is much higher than that of the reflection. This results that the graphene/PMMA microcellular foams with excellent EMI SE would be suitable for the use as electromagnetic absorption materials in the microwave frequency range.

The presence of microcellular cells arranged the brittle graphene/PMMA nanocomposite tough. The addition of graphene sheets made neat PMMA even brittle, evidenced by the reduced ductility and tensile toughness. However, the ductility of the graphene/PMMA nanocomposites is significantly increased after foaming. As shown in Table 2, the PMMA foam with 0.5 wt % graphene sheets gives a fracture strain of 24% compared to 5% for its bulk counterpart, leading to a 346% increment in tensile toughness from 13 to 58 MPa /(kg/m^3). For the foam containing 1.0 wt % graphene sheets, the tensile toughness is increased by more than 3 times. The small cells of the graphene/PMMA microcellular foams are resistant to rupture and favorable for the improvement of toughness. The uniform microcellular cells acted in a similar way as the cavitated rubber particles in rubber-toughened plastics [80].

Table 2: Specific Mechanical Properties of Bulk and Foamed PMMA and Graphene/PMMA Foam (reproduced form Ref. 44)

Sample	Density (g/cm^3)	Specific modulus ($MPa/kg/m^3$)	Specific toughness ($x10^2$) ($MPa/(kg/m^3)$)	Specific strength ($x10^2$) ($MPa/(kg/m^3)$)
neat PMMA	-	1.32 ±0.06	0.46±0.05	48.4±0.3
composite (0.5 wt %)	1.19	1.48±0.13	0.13±0.02	45.5±0.3
composite (1.0 wt %)	1.20	1.56±0.08	0.11±0.07	45.0±0.4
neat PMMA foam	-	0.80±0.04	0.48±0.01	25.2±0.5
composite foam (0.5 wt%)	0.65	0.91±0.04	0.58± 0.06	27.3±2.3
composite foam (1.0 wt%)	0.58	0. 96±0.14	0.47±0.08	28.4±2.6

Before tensile stretching, the microcellular cells showed nearly spherical morphology (Figure 11b). When the foam is subjected to an extension over the tensile yield stress, necking is

observed with severe plastic growth of the microcellular cells near the fracture surface (Figure 11c). The material between voids is plastically stretched and transformed into fibrils (Figure 11d). With the highly stretching, the local stress intensification within the craze eventually enlarged the void content by coalescence of voids. This toughness mechanism of microcellular cells is also reported in PS and PC foams [81,82] and polypropylene nanocomposites with submicrometer voids[83]. In addition, the graphene sheets reinforced PMMA foam with 1.0 wt %, the specific modulus of the PMMA foam increases by 18% and its specific yield strength increases by 13% (Table 2). These improvements are attributed to the reinforcement of cell walls/junctions by the graphene.

Yan, et al [84] reported the development of high loading of functionalized (30 wt. %) graphene sheets (FGS)/ polystyrene (PS) composite foam by a novel compression molding plus salt-leaching method with improved EMI shielding properties. An excellent EMI SE achieved at a relatively high content of electrical nanofiller, which generally restricted by the formation of a porous structure during conventional foam processing because of the remarkable increase in viscosity. The SEM images of FGS/ polystyrene composites of density 0.45 and 0.27 with 30 wt % of FGS with varying the $CaCO_3$ content are depicted Figure 12. It is reported that the porous structure within the composites is fully continuous. The typical open-cell structure is formed throughout the FGS/PS composites, which is attributed to leaching of the $CaCO_3$ in the PS composites (Figure 12a). The light weight composite foam is easily fabricated by increasing the $CaCO_3$ loading, regardless of the nanofiller content. Figure 11b, shows 30 wt% FGS loaded porous FGS/PS composites of density 0.27 g/cm^3. The inset transmission electron micrograph represents that FGSs are dispersed and embedded in the PS system to build an interconnected graphene network (Figure 12a).

EMI SE of the porous FGS/PS composites in the frequency range of 8.2–12.4 GHz is shown in Figure 12 c. The average EMI SE of the 0.45 and 0.27 g/cm^3 samples of 2.5 mm in thickness are 29.3 and 17.3 dB. It has been well established that the EMI SE of conducting composites is mainly related to their electrical conductivity, and increases with the conductivity. The electrical conductivity of the FGS/PS composites of density 0.45 and 0.27 g/cm^3 is reached to 1.25 and 0.22 S/m.

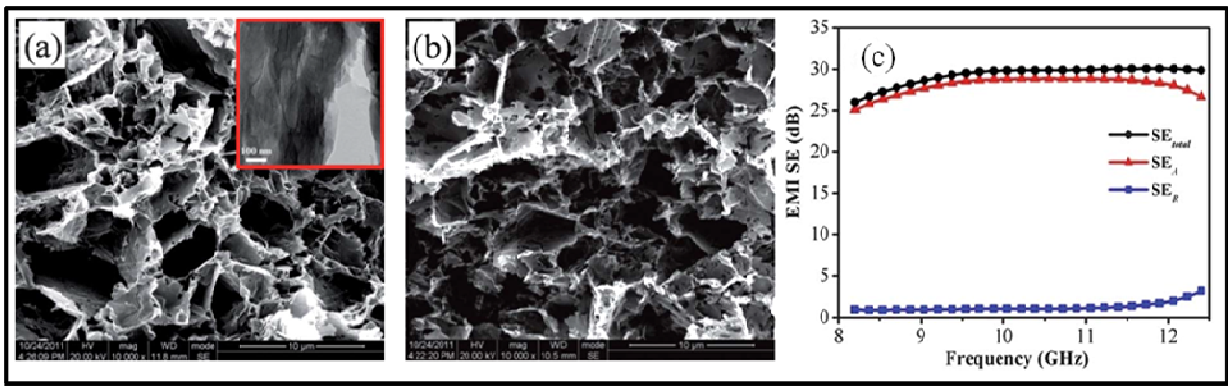

Figure 12: SEM image of FGS/PS composites of density (a) 0.45 g/cc (b) 0.27 g/cc, and (c) EMI SE of FGS/PS of density 0.45 g/cc (Reproduced with permission from ref. 84. Copyright 2012 Royal Society of Chemistry)

The EMI shielding mechanism in the conductive porous FGS/PS composites is investigated and depicted in Figure 12c. The SE is dominated by contribution of microwave absorption and reflection is negligible over the whole frequency range. The average SE_{Total}, SE_A, and SE_R are 29, 27.7 and 1.3 dB for porous FGS/PS of density 0.45 g/cc. This reveals that maximum microwave power is dissipated as heat through the porous composites rather than being reflected back from the composites' surface, which confirms that absorption is the primary EMI shielding mechanism and reflection is the secondary shielding mechanism in the X-band frequency region for such conductive porous composite.

As reported above, chemically derived graphene (CDG)/polymethylmethacrylate(PMMA) composite microcellular foams show a specific EMI shielding effectiveness of 17–25 $dB.cm^3/g$ with a CDG loading of 5 wt% [58]. In addition, CDG has been directly used to fabricate various three-dimensional (3D) macroporous foam structures by self-assembly [85-89]. However, these CDG foam structures also suffer from poor electrical conductivity because of the low quality and/or high inter-sheet junction contact resistance of the CDG sheets. Therefore, their EMI shielding performance is not high. To overcome from this problem, Chen et al [90] reported highly conductive flexible graphene foams with a 3D interconnected network structure using a template-directed chemical vapor deposition (CVD) method, which can be use as a high-performance EMI shielding material. The graphene/polymer foam composite are fabricated by a one-step process without the use of foaming agents, in which the graphene sheets are prepared by CVD and seamlessly interconnected into a 3D network [91]. Graphene is first grown on nickel

foam by CVD of methane at 1000°C under ambient pressure, which copied the structure of the nickel foam and formed a 3D network. Then, a thin layer of PDMS is coated on the surface of graphene. After that, the nickel foam substrate is etched away by HCl, and the graphene/PDMS foam composite is obtained. The content of graphene in the composite and the electrical conductivity of the composite are tuned by changing the flow rate of methane used in the CVD growth of graphene.

The graphene/PDMS foam composite obtained is lightweight, flexible and soft, as shown in Figures 13a. The SEM images confirm that the composite is highly porous and perfectly copies the interconnected 3D network structure of the nickel foam (Figures 13b).

The porosity of the Graphene/PDMS composite is up to ~ 95%, which is much higher than that of the reported composites expanded by foaming agents [36, 44]. This highly porous nature gives the foam composite an ultra low density of < 0.06 g/cm^3, about 20 times lighter than solid polymer composites. Despite its ultra-light weight, the foam composite is highly conductive due to the seamlessly interconnected 3D graphene network providing a fast electron transport channel inside it.

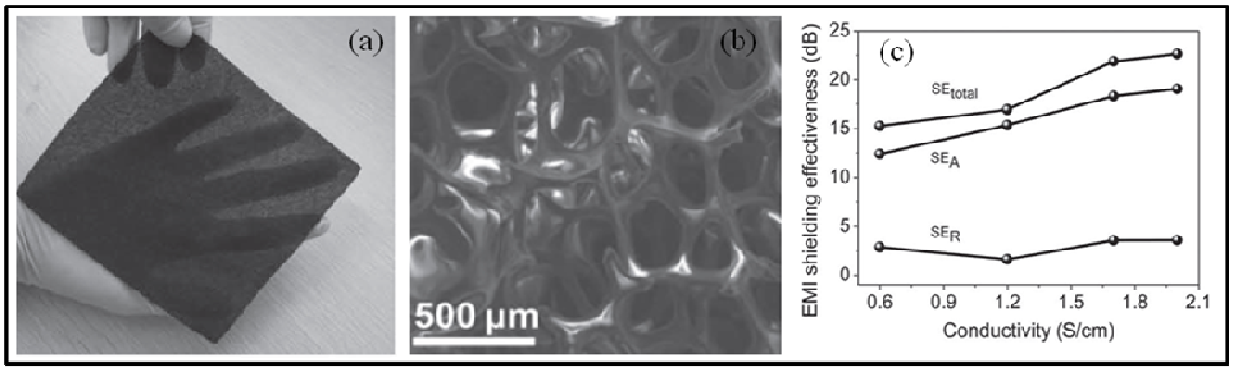

Figure 13: (a) Graphene/PDMS foam composite obtained is lightweight, flexible and soft (b)SEM image of foam composite, showing its 3D interconnected network structure, (c) Comparison of SE_{total}, SE_A and SE_R with different electrical conductivities at frequency 9 GHz (Reproduced with permission from ref. 90. Copyright 2013 Wiley-VCH)

The electrical conductivity of the composite is as high as 2 S/cm with a low graphene loading of < 0.8 wt% which is more than 3 orders of magnitude higher than the conventional CNT and CDG-based polymer composites [36, 44]. Therefore, such lightweight and flexible graphene/PDMS foam composites are expected to show a high EMI shielding performance. The

EMI SE of graphene/ PDMS foam composites with different electrical conductivities measured in the 30 MHz–1.5 GHz and the X-band frequency ranges. The SE increases with increasing loading and electrical conductivity in the same frequency range. The EMI SE of the foam with a conductivity of 1.8 S/cm (< 0.7 wt% graphene) is measured to be ~30 dB over 30 MHz– 1.5 GHz. The composite with a similar conductivity of 2 S/cm (0.8 wt% graphene) shows an EMI SE of ~20 dB in the X-band frequency range. The specific EMI SE of graphene/PDMS foam composites with 0.8 wt% graphene loading can reach ~500 dB cm^3/g in the 30 MHz–1.5 GHz frequency range and ~333 dB cm^3/g in the X-band frequency range. These values are much higher than those of typical metals (10 dB $\cdot$ cm^3/g for solid copper [92]) and carbon/polymer composites (33.1 $dB.cm^3/g$ for foam composites containing 7 wt% CNTs [36]) and 17–25 $dB.cm^3/g$ for foam composites containing 5 wt% CDGs [55]. The superior specific EMI SE is one of the most outstanding advantages of graphene/ PDMS foam composites as a high-performance EMI shielding material, which allows the use of this material in the areas that need light weight materials such as aircraft, spacecraft, automobiles and portable electronics. The different attenuating mechanism behind such high value of EMI SE of the foam composites in X-band is reported.

Figure 13c shows SE_{Total}, SE_A, and SE_R of the graphene/PDMS composites foam as a function of electrical conductivity at 9 GHz. As the electrical conductivity increases, both the SE_{Total} and SE_A increase while SE_R remains almost constant. Moreover, it is importance to note that the contribution of absorption to the EMI SE is much larger than that of reflection. For the foam composite with a conductivity of 2 S/cm, SE_{total}, SE_A, and SE_R are ~ 23, 19 and 4 dB, respectively. For the foam composite with a relatively smaller conductivity of 1.2 S/cm, SE_{Total}, SE_A, and SE_R are ~ 17, 15 and 2 dB. These results suggest that graphene/PDMS foam composites are both reflective and absorptive to EM radiation in the X-band frequency range. The EMI shielding mechanism of foam composites is different from those of carbon nanofibers, multi-wall and single-wall CNT/polymer composites, where reflection is the major contribution to EMI shielding. The two-dimensional structure of graphene as well as the large surface area and interface area in graphene/PDMS foam composites are benefit for the multiple reflection of the incident microwaves inside the foam composites and consequently responsible for the absorption-dominant EMI shielding [44,78]. The excellent flexibility of graphene-PDMS composite foam also gives it a stable EMI shielding performance under mechanical deformation.

It is reported that no degradation in the performance even after repeatedly bending to a radius of ~2.5 mm for 10 000 times. The fabrication of this novel material opens up the possibility for the use of graphene as a lightweight, flexible, and high-performance EMI shielding material in areas such as aerospace and next-generation flexible electronics.

Ling et al [93] reported a facile approach for the development of lightweight microcellular Graphene/Polyetherimide(PEI) composite foams. The Graphene/PEI composite and foams are prepared by a water vapor induced phase separation process (WVIPS) [94] with graphene loading up to 10 wt %. The graphene is used consist of 3-4 sheets and surface area 700 m^2/g [44]. In Table 3 illustrated the density of graphene/PEI nanocomposites foams as a function of graphene content. The density of graphene/PEI foam is 0.28 g/cm^3 and it does not change much with increasing graphene loading up to 10 wt % [93]. In the case of polymer nanocomposite foams blown with physical blowing agent (PBA), however, researchers found that the addition of 9 wt % nanosilica increased the foam density from 0.75 g/cm^3 for pure PC foam to 0.92 g/cm^3 for PC nanocomposite foam, due to the increase in polymer matrix stiffness [95]. Therefore, compared with the microcellular foaming technology using PBA, the WVIPS process exhibited advantage in preparing lightweight polymer nanocomposite microcellular foam.

Table 3: Density and average cell diameter of graphene/PEI composites as function of graphene (reproduced from ref. 93)

Graphene content in nanocomposites (wt%)	Graphene content in nanocomposites (vol %)	Graphene content in foam (vol %)	Foam density (g/cm^3)	Average cell diameter (μ m)
0	0	0	0.28	15.3±4.5
0.1	0.06	0.01	0.29	15.9±4.8
0.3	0.17	0.04	0.28	15.9±3.8
0.5	0.28	0.06	0.28	16.3±5.1
0.7	0.39	0.09	0.28	-
1	0.56	0.12	0.28	16.6±4.9
2	1.13	0.25	0.28	-
3	1.71	0.39	0.29	16.1±4.4
5	2.87	0.75	0.32	13.5±2.5
7	4.05	1.01	0.31	12.1±1.8
10	5.87	1.38	0.29	9.0± 2.0

Figure 14 shows the SEM micrograph of composite foams and Table 3 depicted the average cell diameter. Graphene/PEI foam possessed microcellular cell structure and uniform cell size distribution. The cell size is 16.3 μm with graphene loading of 0.5 wt % and to 16.6 μm with graphene loading of 1 wt %. With a further increase in graphene loading, the cell size in nanocomposites foam tended to decrease to 13.5, 12.1, and 9.0 μm for graphene loading of 5, 7, and 10%, respectively; this is due to the increase in viscosity of dispersion and the physical barrier action of graphene to cell coalescence [96].

For all graphene/PEI nanocomposite foams, the cell size distributions are uniform. The electrical conductivity of PEI is 1.2×10^{-19} S/cm; the addition of graphene increases the electrical conductivity considerably of the compressed graphene/PEI nanocomposites up to 3.9×10^{-10} S/cm with a 1.13 vol % loading, indicating the formation of conductive percolating network among graphene nanosheets. Compared to graphene/PEI nanocomposite, microcellular

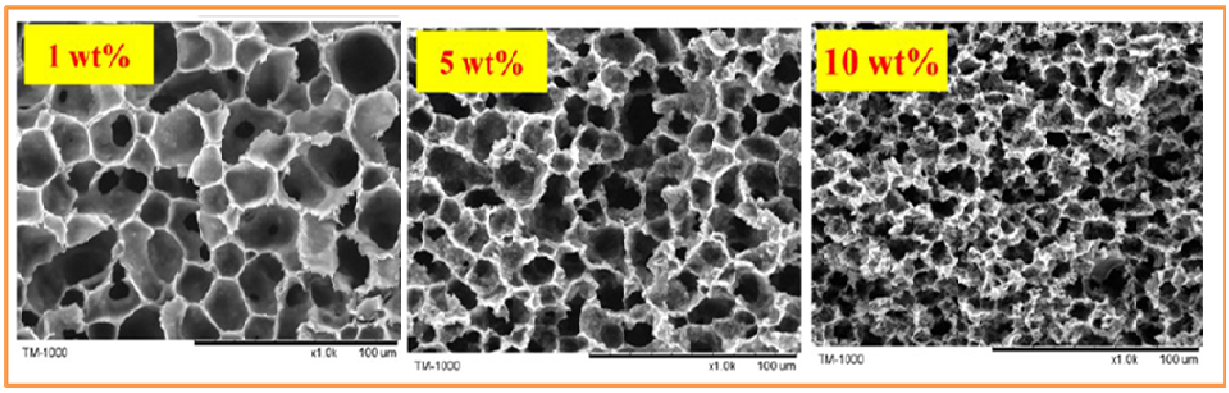

Figure 14: SEM micrograph of PEI-graphene composites as function of graphene content. Reproduced with permission from ref. 93. Copyright 2013 American Chemical Society

Graphene/PEI foam possessed a higher electrical conductivity of 1.75×10^{-8} S/cm with a lower graphene loading of 0.39 vol % loading, which suggested that the presence of microcellular structure might decrease the percolation threshold of the conductive composites. In general, the foaming process presents two effects on the electrical conductivity percolation threshold of polymer nanocomposite. One effect is that the excluded volume related to cell formation pushes nanoparticles together; even more important, the in situ generated strong extensional flow during bubble growth facilitates the orientation of nanoparticles in cell wall [97]. The enriching and orientation of nanoparticles causes the close pack of nanoparticles in the foamed composites. The other effect of the foaming process is the volume expansion, which tends to increase the distance

of adjacent nanoparticles. This demonstrated that the foaming process contributed to a decrease in electrical conductivity percolation threshold from 0.21 to 0.18 vol%, and the volume expansion of foam was about 4 times. This is due to the enrichment and orientation of graphene during cell growth. A further increase in graphene loading gradually increases the electrical conductivity of graphene/PEI nanocomposites up to 4.8×10^{-6} S/cm at graphene loading of 5.87 vol%. In the case of graphene/PEI nanocomposite foams, electrical conductivity rapidly increases up to 2.2×10^{-5} S/cm with the graphene loading of 1.38 vol %. It is reported that graphene/PEI nanocomposite (5.87vol %) and microcellular foams (1.38 vol %) possess the same graphene loading of 10 wt%, which indicated that the microcellular foaming process is a benefit to the improvement of electrical conductivity of graphene/PEI nanocomposites. The EMI shielding of graphene/PEI nanocomposite and microcellular foams in the range of 8-12 GHz is weak frequency dependent; it increases gradually up to 20 dB at 10 wt% graphene loading. After the volume expansion by 4 times in microcellular foam, EMI SE decreases and the value with 10 wt % graphene loading is about 11 dB. The total EMI SE of material includes the contribution of SE_R and SE_A. The SE value of nanocomposite foam is below15 dB, however, SE for graphene nanocomposites is 7.27−19.66 dB at graphene loading of 3−10 wt %, indicating about 76.2−90.8% electromagnetic energy is absorbed by the materials. The introduction of microcellular structure increases the contribution of SE_A to SE_{total}, where about 90.6− 98.9% electromagnetic energy is absorbed by the microcellular foams, suggesting the obvious increase in absorbing ability of samples with the presence of microcellular structure. It is well accepted that the microwave reflection is the result of dielectric mismatch at interfaces. In order to fabricate material with excellent absorption property, the dielectric constant of material must be controlled as close as possible to that of air, i.e.,1. The introduction of tiny air bubbles in polymer matrix by microcellular foaming technology would decrease the dielectric constant without any effect on the component of the matrix [98]. In addition to this spherical microscale air bubbles in the foams attenuate the incident electromagnetic microwaves by reflecting and scattering between the cell wall and nanofillers, and the microwaves are difficult to escape from the sample before being absorbed and transferred to heat [99]. This microcellular foam is idea to decrease the reflection of microwaves makes polymer nanocomposite an excellent microwave absorber compared with the bulk shielding composite.

In another study, Shen et al [100] presented high performance graphene@Fe_3O_4 /PEI composite foam with low density and improved EM absorption properties. The chemically derived graphene are functionalized by biocompatible and low toxicity Fe_3O_4 nanoparticles which is contributing the high complex permeability to graphene (G) due to the large saturation magnetization [101]. The G@ Fe_3O_4 /PEI composite foam are prepared by water vapor induced phase separation process [102] with varying the G@Fe_3O_4 from 0 to 10 wt % in which graphite oxide and Fe_3O_4 ratio 1:1. The G@ Fe_3O_4 hybrid is prepared by chemical deposition of iron onto graphite oxide sheets and then chemical reduction of graphite oxide with hydrazine. The density of G@Fe_3O_4 /PEI foam is about 0.28−0.40 g/cm^3 at 1.0−10.0 wt % loading. Figure 15a, shows the typical optical image of the foams with G@Fe_3O_4 loading of 5.0 and 10.0 wt %. It is demonstrated that foam sheets are quite flexible under bending. The corresponding SEM images of fracture surfaces are depicted in Figure 15a; it shows the uniform microcellular cell structures are formed in foams at lower G@Fe_3O_4 loading of 5 wt %. This unique structure is ascribed to the occurrence of phase separation due to the diffusion of water vapor into the composite solution. While in 10.0 wt % loading induced the formation of the bimodal distribution of cell structures (small cells existed around the big cell), because of the enhanced viscosity of suspension and the aggregation of G@Fe_3O_4 at higher contents [103].

The EMI SE of G@Fe_3O_4/PEI foams with a thickness of 2.5 mm in X-band (8−12 GHz) increases with increasing the G@Fe_3O_4 loading content. The SE of all the foams exhibited weak frequency dependency in the measured bands. The EMI SE of the foam with 1.0 wt % G@ Fe_3O_4 is 3.5−5.8 dB and an increase of G@Fe_3O_4 content to 5.0 wt %, the EMI SE value is vary from 6.5 to 9.2 dB. The EMI SE value increases up to 14.3−18.2 dB for the foam with 10.0 wt % G@Fe3O4.

To clarify the EMI shielding mechanism in G@Fe_3O_4/PEI foams, the SE_{total} , microwave reflection (SE_R) and microwave absorption (SE_A) at 9.6 GHz from the measured scattering parameters (S11 and S21) is reported. It reveals that the increase in G@ Fe_3O_4 loading led to the enhancement of both SE_{total} and SE_A and the contribution of SE_R is negligible for all of the microcellular foams with different G@Fe_3O_4 loadings. For example, the SE_{total}, SE_A, and SE_R are 13.1, 12.7, and 0.4 dB for the foam with 7.0 wt % G@Fe_3O_4, whereas the corresponding values are 17.8, 17.3, and 0.5 dB for the foam with 10.0 wt % G@Fe_3O_4. This reveals that most of microwave power is dissipated as heat through the microcellular foams rather than being

reflected back from the surface of the foam, which confirmed that absorption is the main EMI shielding mechanism. This phenomenon is depicted in figure 14b; the microcells in the G@Fe_3O_4/PEI foams provided a large cell-matrix interface area. The incident electromagnetic waves entering the composite foam could be repeatedly reflected and scattered between these interfaces, and they are hard to escape from the composite foam until being dissipated as heat. Moreover, the layered structure and large aspect ratio of G@Fe_3O_4 hybrid may also cause the multiple reflections. As demonstrated in Figure 15c and 15d, the two parallel G@Fe_3O_4 sheets may reflect and scatter the incident electromagnetic waves many times between the sheets inside, increasing their propagation paths in the composite foam, which could further enhance the absorbing ability. Another factor that contributes to microwave absorption is impedance matching.

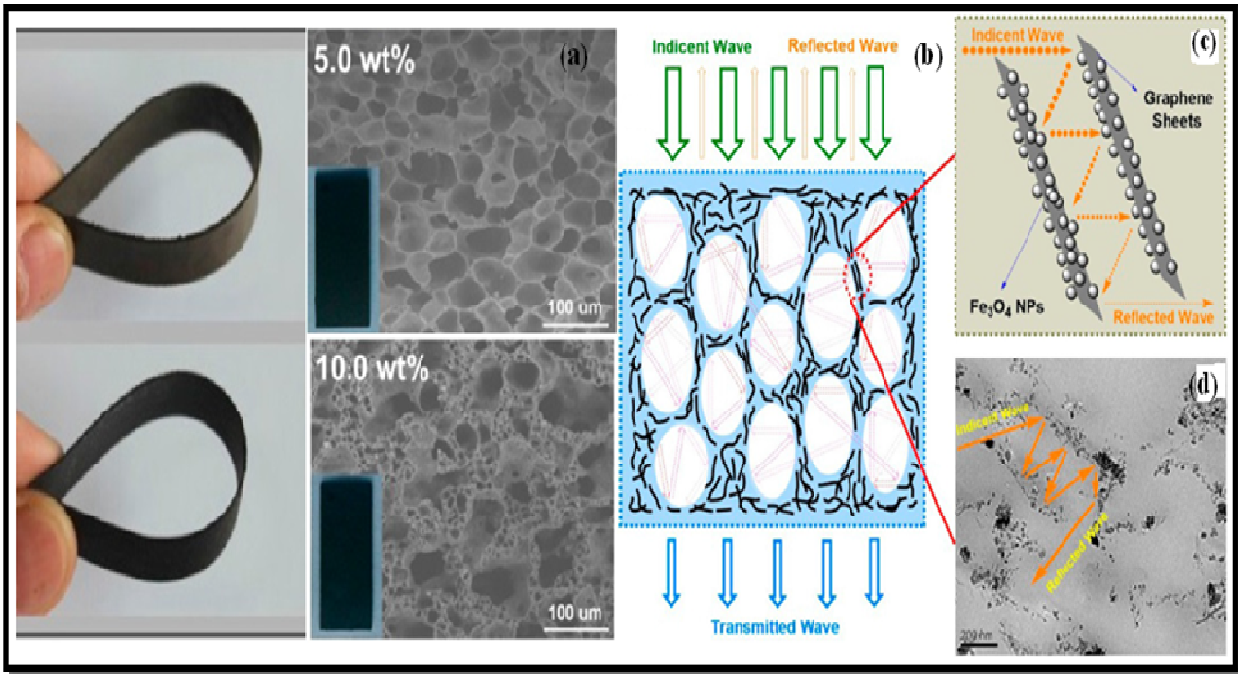

Figure 15: (a) Optical and SEM micrograph of foam with 5 and 10 wt% G@Fe_3O_4, (b) schematic description of electromagnetic wave transfer across the PEI/G@Fe_3O_4 foams; (c) schematic diagram representing the multi reflection route of electromagnetic wave between the G@Fe_3O_4 sheets; (d) TEM image showing two parallelG@Fe_3O_4 sheets in the matrix as well as the possible reflection path of electromagnetic wave (Reproduced with permission from ref. 100. Copyright 2013 American Chemical Society)

.

The DC electrical conductivity of the G@Fe_3O_4/PEI foams is lower than that of the PEI/graphene foams [93]. This suggest that the introduction of Fe_3O_4 nano particles tended to decrease the electrical conductivity of the composite foams, which would improve the equality of the EM parameters, and thus improve the level of impedance matching and decrease the surface reflection [104]. Another factor that contributes to microwave absorption is EM wave attenuation, determined by dielectric loss and magnetic loss [105-106]. It is well known that electronic, ionic, orientational and space charge polarization determines the total dielectric property of the material. In a heterogeneous system, the accumulation of virtual charges at the interface of two medium with different conductivities and dielectric constants would lead to interfacial polarization and is known as Maxwell−Wagner polarization. Pristine graphene is nonmagnetic and contributes to microwave absorption mostly due to its dielectric loss. The introduction of Fe_3O_4 on graphene sheets would not only enhance the magnetic losses but also enhance the dielectric losses in a wide frequency range, resulting from the interfacial polarizations between the Fe_3O_4 and graphene because of the formation of a heterogeneous system and more interfaces, as well as the stronger coupling at the gaps between the neighboring Fe_3O_4 [105]. Also, the presence of oxygen groups and defects on the reduced graphene could help to improve the microwave absorption of the composite foams [107]. This technique is fast, highly reproducible, and scalable, which may facilitate the commercialization of such composite foams and generalize the use of them as EMI shielding materials in the fields of spacecraft and aircraft.

Recently, Bernal et al [108] has discussed about rigid polyurethane (PU) nanocomposite foams filled with 0.17 and 0.35 wt% MWCNTs, functionalized MWCNTs (f-MWCNTs) and functionalized graphene sheets (FGS). The effect of different content of carbon nanoparticles on foam morphology and EMI SE properties of composites foam is reported. The electrical properties of rigid PU nanocomposite foams are strongly dependent on the foaming evolution, cellular structure and density of these materials, which are them self influenced by the morphology, aspect ratio and surface functionlization of the carbon-based nanofillers. The morphology of foams is determined by the reaction rate which controls the production of gas and the evolution of the fluid rheology [109]. It is considered that in reactive foams two phases govern the foaming dynamics and hence the morphological development: the continuously

polymerizing liquid matrix and the disperse gas phase [110]. Both phases are strongly influenced by several parameters (e.g. rate of gas production, diffusivity) being surface tension, temperature, viscosity important on the bubble growth formation and stability. The temperature increases, both viscosity and surface tension decrease, and then membranes become thinner and in some cases rupture because they cannot support the polymer stresses [111-112]. Besides these parameters, in reactive polyurethane nanocomposite foams, two other competing effects influence the cell diameter i.e. the blowing effect, which increases the cell diameter and the nucleation effect which decreases the cell diameter. The blowing effect is produced by the presence of water on the surface of the nanoparticles. Meanwhile, the nucleation effect depends on the degree of dispersion of nano fillers in the polymer matrix [113]. The structure of rigid PU nanocomposite foams is demonstrated in (Figure 16) and the average cell size is summarized in Table 4. It is widely known that hydrophobic particles can cause instability, producing the rupture of the cells. However, the particles are well-dispersed in the system; they increase the bulk viscosity and thus can cause an increase of the stability [114,115]. In addition, the effective stabilization mechanism is higher as the particle size is smaller [116]. In rigid PU foams filled with MWCNTs a good dispersion of the nanotubes is achieved in the initial system increasing the bulk viscosity which slows down the drainage rate, preventing the rupture of the cells [114-115] Hence, even there is increase in the temperature of the reaction during the foaming, the high viscosity is enough to withstand the polymer stresses on the cell walls maintaining the cell structure [112,117]. Therefore, the clear reduction of the cell diameter (Table 4), as the content of nanoparticles increases, confirms the nucleation effect of MWCNTs on rigid PU foams. On the other hand, rigid PU foam filled with low contents of f-MWCNTs and FGS show similar cell diameters as 0.17 wt% of MWCNTs. For high contents (0.35 wt %) of f-MWCNTs, the cell diameter is similar to that of neat rigid PU foam. This increase in the cell size as a function of loading fraction suggests that the blowing effect is dominant for these foams due to the hydrophilic nature of f-MWCNTs. In the case of FGS larger loading fractions (0.35 wt%), results in an increase of the cell diameter although less pronounced than in rigid PU foams with f-MWCNTs, because the content of the hydrophilic groups on the surface of the graphene sheets is lower. In addition, for rigid PU foams filled with high contents of FGS and f-MWCNTs, it is observed (Figure 15) that a broad distribution of the cell size, which is related to coalescence effects. The lower viscosity of the initial dispersions of f-MWCNTs and FGS causes instability

because of the stresses generated in the cell walls by the polymer and the nanoparticles, collapsing the cell structure.

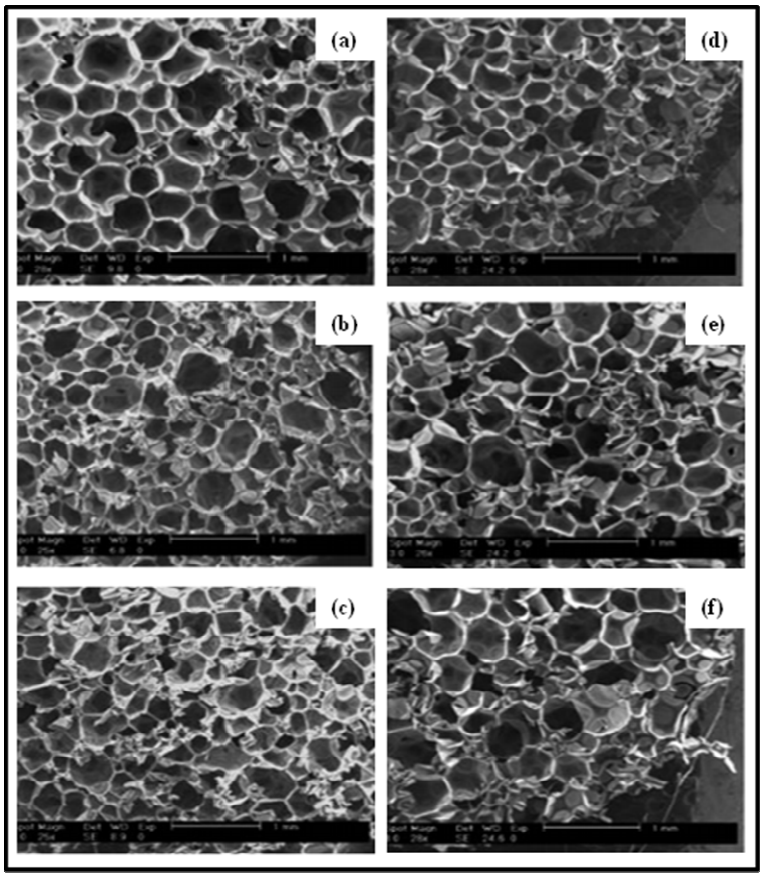

Figure 16: SEM images of PU nanocomposite foams with 0.17 wt% (a) MWCNTs, (b) f MWCNTs, and (c) FGS; 0.35 wt% (e) MWCNTs, (f) f-MWCNTs, and (g) FGS. (Reproduced with permission from ref. 108. Copyright 2014 Royal Society of Chemistry)

Table 4: PU nanocomposite foam cell size, density and specific SE with different nanoparticle content (reproduced ref. 108).

Sample	Cell size (μm)	Density (kg/m^3)	Cell wall thickness (μm)	Cell density ($n.cm^{-3}$)	Specific SE $dB\ cm^3/g$
Neat	545±12	82.4±0.4	20.5	1.52×10^5	4
MWCNTs 0.17 wt %	442±19	75.3±06	15	3.00×10^5	
MWCNTs 0.35 wt %	359±10	70.9±3.5	12	5.50×10^5	38.7
fMWCNTs 0.17 wt %	424±48	71.9±2.6	14	3.75×10^5	
fMWCNTs 0.35 wt %	533±55	58.2±1.5	14	2.52×10^5	12.5
FGS 0.17 wt %	427±17	65.1±2.3	12.5	4.25×10^5	
FGS 0.35 wt %	476±43	58.2±0.9	12.5	3.55×10^5	9.8

Figure 17 shows the variation in electrical conductivity and specific EMI SE nanoparticles loaded PU foam with increasing frequency. As it is expected, the presence of nanoparticles increases the values of conductivity and specific EMI SE, and it almost independent of the frequency X band region. While the average value specific SE for neat rigid PU foam is approximately 4 dB cm^3/ g, the inclusion of 0.35 wt% of f-MWCNTs and FGS, it increases to around 12.5 and 9.8 dB cm3/g (Figure 17b). While, in MWCNT –PU foam the specific EMI SE is more or less frequency dependent and the maximum value achieved for 0.35 wt% at 12 GHz is around 38.7 dB cm^3/g. The increase in EMI SE is attributed to an increase in conductivity of the nanocomposites foams (Figure 17a). The conductivity increases by two orders of magnitude for foams with 0.35 wt% of MWCNTs and by one order for f-MWCNTs and FGS compared to the neat foam. Hence, raw MWCNTs form a better conductive network than f-MWCNTs and FGS in rigid PU nanocomposite foams.

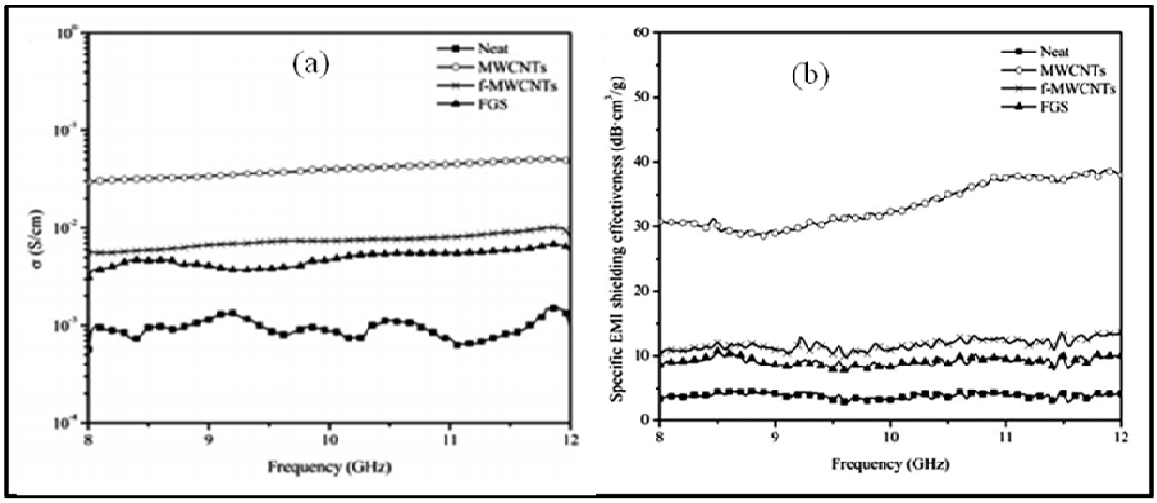

Figure 17: (a) Conductivity and (b) specific shielding effectiveness of nanoparticle filled PU composite foam (Reproduced with permission from ref. 108. Copyright 2014 Royal Society of Chemistry)

As a result, the explanation to the observed results is the combination of two different aspects: (i) the morphology and functionalization of carbon nanoparticles and (ii) the cellular structure of the final foams. Foams with f-MWCNTs presented lower values of EMI shielding and conductivity than the ones with MWCNTs, which is ascribed not only to the lower aspect ratio of f-MWCNTs but also to the oxygen-bearing groups of their surface, creating defects on the crystalline

structure of the carbon nanotubes and hence reducing the number of p-electrons. The same effect was observed on foams filled with FGS where the presence of functional groups on their surface prevents the high electronic transport of π-electrons [118] On the other hand, the cellular structure of the final foams plays a key role on the EMI SE of these polymer materials. Rigid PU nanocomposites foams with higher density and less collapsed structure favors the formation of a better conductive pathway due to an increase of the number of contacts between the nanoparticles [119] as it is observed for foams filled with MWCNTs.

Li et al. [120], reported the EMI shielding properties of rGO- polyimide (PI) composite foams with increasing the rGO content from 1 to 16 wt%. The composite foam was developed by a three-step method: in situ polymerization, nonsolvent induced phase separation and thermal imidization. Figure 18a demonstrated the EMI SE of the foams in the X-band frequency region and EMI SE is almost independent of frequency. The addition of 8 wt% rGO in the PI, the SE of the foam varies from 7.5 to 11.1 dB. The value increases to 11.7–15.3 dB when rGO loading is increases up to 12 wt%. The highest SE is 17.0–21.1 dB for the foam with 16 wt% rGO. Figure 18 b shows the different contribution of SE (SE_{total}, SE_R, SE_A). The increase in rGO loading leads to the enhancement of S_{Etotal} and SE_A contributed mostly to the SE_{total}. The SE_{total}, SE_A, and SE_R at 9.6 GHz were 10.4, 9.9, and 0.5 dB for the foam with 8 wt% rGO, whereas the corresponding values for the foam with 16 wt% rGO were 20, 17.6, and 2.4 dB, respectively. This revealed that EMI shielding mechanism is dominated by absorption rather than reflection. Specially, the ratio of SE_A to SE_{total} decreases gradually from 95.2% for the 8 wt% rGO/ PI foam to 88.0% for the 16 wt% rGO/ PI foam, suggesting the decrease absorbing ability of the foams with increasing rGO content.

The resultant 16 wt% rGO/ PI foam with low density of 0.28 g/cm^3 and thickness of 0.8 mm exhibited an effective EMI SE of 17–21 dB (specific shielding 75dB cm^3/g in X band). Additionally, thermal stability of the rGO-PI foams is also significantly increases. It is reported that up to 508° C, there is 5% weight loss in pure PI foam while the same weight loss in rGO-PI composite foam at 581°C with 16 wt% rGO content. This suggests that there is increase in the thermal stability by 80°C in rGO-PI foam. Even with the high rGO content (16 wt%), the composite foam was fairly flexible.

To get first hand information about the work carried out on carbon nanomaterials filled polymer composites foam as EMI SE material are depicted in table 5.

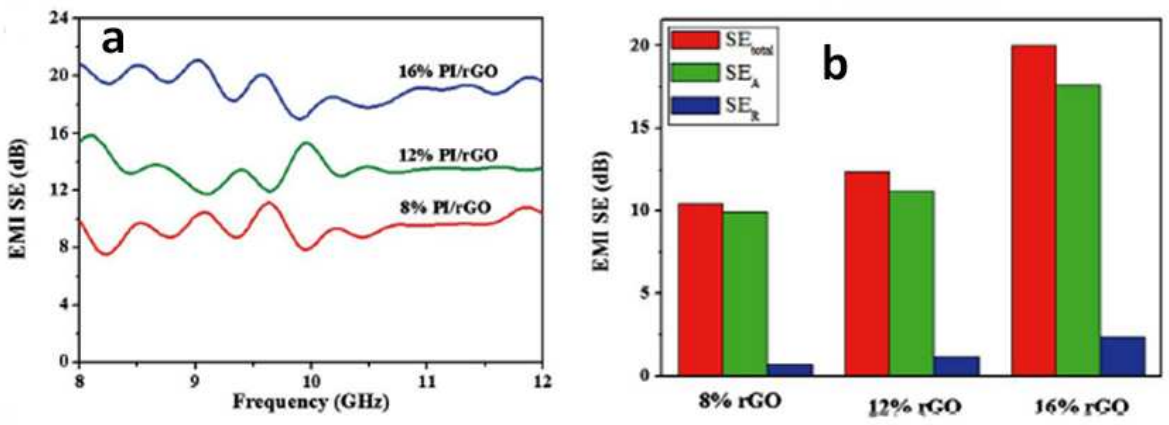

Figure 18 (a) EMI SE of rGO/PI foam with different rGO contents in X-band and (b) the corresponding S_{Etotal}, SE_A and SE_R at 9.6 GHz. (Reproduced with permission from ref. 120. Copyright 2015 Royal Society of Chemistry)

Table 5: Carbon nanomaterials filled polymer composites foam as EMI SE material

Filler	polymer	Filler content and size	Density g/cc	SE_T (dB)	SE_R (dB)	SE_A (dB)	Ref.
nanofiber	PS	15 wt %, dia.100-200 nm Length 30-100 µm	0.56	-19	-	-	36
MWCNT	PS	7wt%, dia. 10-20 nm Length 5-20 µm	0.56	20	16.2	3.6	37
MWCNT	PU	2wt %	0.05	-	-	-	38
MWCNT	PCL	0.25 vol.%	0.31	60	8	52	39
SWCNT	PPHIPE	0.1 wt%	0.87				
MWCNT	FC	0-12 wt %	1.2	5-42			43
MWCNT	PU	0.35 wt%	0.71	27.5	-	-	108
FMWCNT	PU	0.35 wt %	0.58	7.25	-	-	108
FGS	PVDF	5wt% ,thick 2-5nm, Length 20-40 µm		20	16	4	47
FLG	PMMA	1.8 vol %, 3.4 layers	0.79	19	1	18	44
FGS	PS	30wt%	0.45	29	1.3	27.7	84
CVDG	PDMS	<0.8 wt%	0.06	23	4	19	90
FLG	PEI	1.38 vol%, 3-4 graphene layer	0.29	13	1.5	11.5	93
FLG-Fe_3O_4	PEI	10wt% G@Fe3O4	0.40	17.8	0.5	17.3	100
FFGS	PU	0.35 wt%	0.58	5.68	-	-	108
rGO	Polyimide(PI)	1 to 16 wt%	0.28	17-21			120

5. Summary

In this review, we have systematically outlined the recent progress related to carbon nanomaterials filled polymer nanocomposites light weight, corrosion resistance, flexible, and low cost foam as an efficient EMI shielding material mostly in X-band frequency region. In most of the studies it is reported that EMI SE of the carbon nanomaterials filled polymer composite foams are dominated by reflection phenomena due to the high value of electrical conductivity. While there are some exciting results are presented at low loading of MWCNTs in polymer composite foam. It is demonstrated that, if the cell size and cell density is control in the composite foam then shielding efficiency as high as 60 to 80 dB in the frequency range 26–40 GHz together with a low reflectivity at a 0.25 vol % of CNTs loading. This type of shield material required as an EM radiation absorbers in radar and satellites application that operate in Ka band frequency region.

On the other hand, single atom thick or few layer thick graphene filled polymer nanocomposites foam demonstrated as promising material for EMI shield. The CVD derived graphene- polymer composites foam specific SE (333dB cm^3 /g) is surpassed best values for metal and carbon based composite material. The SE is mostly dominated by adsorption of EM radiation rather than reflection. The two-dimensional structure of graphene as well as the large surface area and interface area in graphene foams are benefit for the multiple reflections of the incident radiation as well as scattering of wave many times between cell-matrix interfaces. The excellent flexibility of graphene composite foam also gives it a stable EMI shielding performance under mechanical deformation. The flexible graphene foam can be used as shield material in the areas that need light weight materials such as aircraft, spacecraft, automobiles, portable electronics and sheath technology particularly unmanned vehicle etc. In spite of considerable progress there is a need to improve the shielding properties of flexible graphene –polymer composite foam to be used in commercial applications. We presume that more work on light weight composite foam is required to promoting further developments in this interesting area of research achieving considerable progress as efficient shielding material for different high end applications.

Acknowledgments

Authors are highly grateful to Director, CSIR-NPL, for his kind permission write a review article and publish the same. Also like to thanks Dr. A.M. Biradar, Head, Division of Materials Physics and Engineering, NPL, New Delhi.

References

1. D.D.L. Chung, *Carbon* 2001,**39**, 279–285.

2. R. Kumar, S. R. Dhakate, T. Gupta, P. Saini, B. P. Singh, R. B. Mathur, *J. Mater. Chem. A,* 2013,**1**, 5727-35.

3. S. Shinagawa, Y. Kumagai, K.Urabe. *J Porous Mater* 1999,**6(3)**,185–90.

4. J. Hajdu, *Trans Inst Metal Finish* 1997,**75**,B7–B10

5. N.V. Mandich, *Plating & Surface Finish* 1994,**81(10),**60–63.

6. L.L. Wang, B. K. Tay, K.Y. See, Z. Sun , L.K. Tan, D. Lua, Carbon 2009, 47, 1905-1910

7. J. Ziaja, M. Ozimek, J. Janukiewicz. (2010).Electrotech. Rev. 2010, R.86, 222-224

8. Ziaja Jan and Jaroszewski Maciej (2011). EMI Shielding using Composite Materials with Plasma Layers, Electromagnetic Waves, Prof. Vitaliy Zhurbenko (Ed.), ISBN: 978-953-307-304-0, InTech, Available from: http://www.intechopen.com/books/electromagnetic-waves/emi-shielding-using-composite-materials-withplasma- layers

9. N. C. Das, D. Khastgir, T. K. Chaki and A. Chakraborty, *Composites, Part A*, 2000, **31**(10), 1069–1081.

10.A. Kaynak, A. *Mater. Res. Bull.* 1996, **31**, 845.

11. T. K. Gupta, B. P. Singh, S. R. Dhakate, V. N. Singh and R. B. Mathur, Journal of Materials Chemistry A, 2013, 1, 9138-9149.

12. K.B. Cheng, S. Ramakrishna, K.C. Lee, *Composites, Part A* 2000, **31**, 1039.

13. Lee, B. O.; Woo, W. J.; Kim, M. S. *Macromol. Mater. Eng.* 2001,***286*****,** 114.

14. A. S. Babal, R. Gupta, B.P. Singh,V.N. Singh, S.R. Dhakate, R.B.Mathur, RSC Advances, 2014, 4, 64649-64658.

15. Wojkiewicz, J. L.; Fauveaux, S.; Miane, J. L. *Synth. Met.* 2003, **127**, *135-136*.

16. B.P. Singh, K. Saini, V. Choudhary, S. Teotia, S. Pande, P. Saini and R. B.Mathur, Journal of nanoparticle research, 2014, 16, 1-11

17. Chen, H. C.; Lee, K. C.; Lin, J. H. *Composites, Part A* 2004, ***35***,1249.

18. B. P. Singh, P. Saini, T. K. Gupta, P. Garg, G. Kumar, I. Pande, S. Pande, R. K. Seth, S. K. Dhawan and R. B. Mathur, Journal of Nanoparticle Research, 2011, 13, 7065-7074.

19. R.A. Tellakula, V.K. Varadan, T.C. Shami, G.N. Mathur, *Smart Mater. Struct.* 2004, 13, 1040.

20. D. Chen , J. Yang , G.Chen, *Comp Part A* 2010, **41(11),**1636–8.

21. Q.J. Krueger, J.A.King, *Adv Polym Technol* 2003,**22(2)**, 96–111.

22. T.K. Gupta, B.P. Singh, Satish Teotia, Varun Katyal, S.R. Dhakate, RB Mathur, J Polymer Research 2013,**20**,1-7.

23. N.C.Das, D. Khastgir, T.K. Chaki, A. Chakraborty, *Comp Part A* 2000,**31(10)**, 1069–81.

24. www.chomerics.com.

25. www.boeing.com

26. H. Chang, M.J. Kao, K.D.Huang, C.G. Ku, S.Y.J Huang, *Nanoscience Nanotechnology* 2011, **11(2),** 1754-7.

27. R. Ramasubramanjam, J. Chen, H. Liu, *Appl. Phys. Lett.* 2003, **83,** 2928.

28. Y.L.Yang, M.C. Gupta, K.L. Dudley, R.W. Lawrence, *Nanotechnology* 2004, **15**,1545.

29. H.J. Barraza, F. Pompeo, E.A.O'Rear, D.E. Resasco, *Nano. Lett.* 2002, **2**, 797.

30. H.M. Kim, K. Kim, C.Y. Lee, J. Joo, S.J. Cho, H.S. Yoon, D.A. Pejakovic, J.W. Yoo, Epstein, A. J. *Appl. Phys. Lett.* **2004**, *84*, 589.

31 Y.L. Yang, M.C. Gupta, K.L. Dudley, R.W. Lawrence, *J. Nanosci. Nanotechnol.* 2005, ***5*,** 927.

32. J.C. Grunlan, A.R. Mehrabi, M.V. Bannon, J.L. Bahr, *Ad*v. *Mater.* 2004, ***16*,** 150.

33.D.-X. Yan, P.-G. Ren, H. Pang, Q. Fu, M.-B. Yang and Z.-M. Li, *Journal of Materials Chemistry*, 2012, **22**, 18772-18774.

34.R. Kumar, S. R. Dhakate, P. Saini and R. B. Mathur, *RSC Advances* 2013,**3**, 4145-4151.

35. X. Han and Y. Wang, *J Functional Materails and devices* 2007, **13**, 529.

36. Y.L. Yang, M.C. Gupta, K.L. Dudley, R.W. Lawrence, Advanced Materials 2005, **17(16)** 1999-2003

37.Y. Yang, M.C. Gupta, K.L. Dudley, R.W. Lawrence, Nano letters, 2005,**11**, 2131-2134.

38. X.B. Xu, Z.M. Li, Lei Shi, X.C. Bian and Z.D. Xiang, Small 2007,**3(3),** 408–411.

39. J. M. Thomassin, C. Pangoulle, Lukasz Bednarz, I. Huynen, R. Jerome, C. Detrembleur, J. Mater Chem 2008,**18**, 792-796.

40. A. Saib, L. Bednarz, R. Daussin, C. Bailly, X. Lou, J.-M. Thomassin, C. Pagnoulle, C. Detrembleur, R. Jerome and I. Huynen, IEEE Trans. Microwave Theory Tech., 2006, **54**, 2745–2754.

41. A. N. Lagarkov and A. K. Sarychev, Phys. Rev. B, 1996, **53**, 6318–6336.

42. M. C. Hermant, B. Klumperman and C. E. Koning, Chemical Communication, 2009, **19**, 2738- 2740.

43. A. Fletcher, C. Gupta, K.L. Dudley, E. Vedeler, Composites Science and Technology 2010, **70(6),** 953-958.

44.H.B. Zhang, Q.Yan, W.G. Zheng, et al. Appl Mater Interfaces2011, **3**, 918–924.

45. J.M. Thomassin, C. Pagnoulle, L. Bednarz, et al. J Mater Chem2008, **18**, 792–796.

46. I.Huynen, N.Quie´vy, C. Bailly, et al. Acta Mater2011, **59**, 3255–3266.

47. L. Chen, D. Rende, L.S. Schadler , R. Ozisik, J. Mater Chem A, 2013, **1**, 3837-3850

48. L. Chen, R. Ozisik, L.S. Schadler, Polymer 2010, **51**,2368–2375.

49. C. Zeng, N. Hossieny, C. Zhang, et al. Polymer2010 **51**, 655–664.

50. R. Rizvi, J.K. Kim, H. Naguib, Smart Mater Struct2009, **18,** 104002.

51. Y.H. Kim, W. Li, , Journal of Cellular Plastics 2013, **49**, 2 131-145.

52. C. Zhou, P. Wang, W. Li, Compos Part B: Eng2011, **42**, 318–325.

53. W. Bauhofer, J.Z. Kovacs, Compos Sci Technol 2009, **69**, 1486–1498.

54. D.I. Collias, D.G. Baird, R.J.M. Borggreve, Polymer 1994,**35**, 3978-83.

55. D.L.Tomasko, H. Li, D. Liu, X. Han, M.J. Wingert, L.J. Lee, et al. Ind Eng Chem Res 2003, **42**,6431-56.

56. V .Kumar, Cell Polym 1993, **12**,207-23.

57. V. Kumar, Prog Rubber Plast Technol 1993, **9**,54-70.

58. M-P Tran, C. Detrembleur, M. Alexandre, C. Jerome, J-M Thomassion, Polymer 2013, 54, **13**,3261-3270.

59. Fletcher NH. J Chem Phys 1958, **29**, 572e6.

60. Shen J, Zeng C, Lee LJ. Polymer 2005, **46**, 5218e24.

61. D. Rende, L.S. Schadler, R. Ozisik, Journal of Chemistry 2013,Article ID 864926, pages 13.

62.L.J. Lee, C. Zeng, X. Cao, X. Han, J. Shen, G. Xu. Compos Sci Technol 2005,**65**,2344-63.

63. A. M. K. Esawi, M.M. Farag, Mater. Design 2007, **28**, 2394–2401.

64. A. Ameli, M. Nofar, C.B. Park, P. Po¨ tschke, G. Rizvi, Carbon, 2014, **71**, 206 –217

65. D. Li, M.B. Muller, S. Gilje, R.B. Kaner, G.G. Wallace, Nat. Nanotechnol. 2008**, 3**, 101-105.

66. S. Stankovich, D. A. Dikin, G. H. B. Dommett, K. M. Kohlhaas,E. J. Zimney, E.A. Stach, R. D. Piner,S. T. Nguyen, R. S. Ruoff, Nature 2006, **442**, 282.

67. V. Eswaraiah, V. Sankaranarayanan, S. Ramaprabhu, Macromolecluar Materials and Engineering 2011, **296**(10), 894-898.

68. A. Kaniyoor, T. T. Baby, S. Ramaprabhu, J. Mater. Chem. 2010, **20**, 8467.

69. V. Eswaraiah, V. Sankaranarayanan, A. K. Mishra, S. Ramaprabhu, International Conference on Chemistry and Chemical Engineering (ICCCE), 2010, 150.

70. Lee, L. J.; Zeng, C. C.; Cao, X.; Han, X. M.; Shen, J.; Xu, G. J. Compos. Sci. Technol. 2005, **65**, 2344–2363.

71. Zeng, C. C.; Han, X. M.; Lee, L. J.; Koelling, K. W.; Tomasko, D. L. Adv. Mater. 2003, **15**, 1743–1743.

72. F. Yavari, M. A. Rafiee, J. Rafiee, Z.Z. Yu, N. Koratkar, ACS Appl. Mater. Interfaces 2010, **2**, 2738–2743.

73. S. Stankovich, D.A. Dikin, G.H. B. Dommett, K.M. Kohlhaas, E.J. Zimney, E. A.Stach, R.D. Piner, S.T. Nguyen, R.S. Ruoff, Nature 2006, **442**, 282–286.

74. H. Kim, K. Kim, C. Y. Lee, J. Joo, S.J. Cho, H.S. Yoon, D.A. Pejakovi_c, J.W. Yoo, A. J. Epstein, Appl. Phys. Lett. 2004, **84**, 589–591.

75. B. Fugetsu, E. Sano, M. Sunada, Y. Sambongi, T. Shibuya, X. Wang, T. Hiraki, Carbon 2008, **46**, 1256–1258.

76. B.W. Li, Y. Shen, Z.X. Yue, C. Nan, Appl. Phys. Lett. 2006, **89**, 132504.

77. V. Choudhary, S.K. Dhawan, P. Saini, Polymer based nanocomposites for electromagnetic interference (EMI) shielding EM Shielding – Theory and Development of New Materials, 2012: ISBN: 978-81-308-0499-6

78. M.H.Al-Saleh, U. Sundararaj, Carbon 2009, **47,** 1738–1746.

79. J.C. Wang, C.S. Xiang, Q. Liu, Y.B. Pan, J.K. Guo, *Adv. Funct. Mater*. 2008, **18**, 2995–3002.

80. A. Dasari, Z. Z.Yu, Y. W. Mai, *Polymer* 2009, **50,** 4112–4121.

81. D.I. Collias, D.G. Baird, *Polym. Eng. Sci*. 1995, **35**, 1167–1177.

82. D.I. Collias, D.G. Baird, R.J. M. Borggreve, *Polymer* 1994, **35**, 3978–3983.

83. A. Dasari, Q.X. Zhang, Z.Z. Yu, Y. W. Mai, *Macromolecules* 2010, **43**, 5734–5739.

84. D. X. Yan, P.G. Ren, H. Pang, Q. Fu, M.B. Yang, Z.M. Li, *J. Mater. Chem*. 2012, **22**, 18772−18774.

85. C. Li , G. Q. Shi , *Nanoscale* 2012 , ***4*** , 5549 .

86. S. Y. Yin , Z. Q. Niu , X. D. Chen , *Small,* 2012 , ***8*** , 2458 .

87. S. H. Lee , H. W. Kim , J. O. Hwang , W. J. Lee , J. Kwon , C. W. Bielawski , R. S. Ruoff , S. O. Kim , *Angew. Chem. Int. Ed.* 2010 , ***49*** , 10084 .

88. Y. Xu , K. Sheng , C. Li , G. Shi , *ACS Nano* 2010 , ***4*** , 4324 .

89. Z. Q. Niu , J. Chen , H. H. Hng , J. Ma , X. D. Chen , *Adv. Mater.* **2012** , *24* , 4144 .

90. Z. Chen, C. Xu, C. Ma, W. Ren,H-M. Cheng, Advanced Materials 2013,25,1296-1300.

91. Z. P. Chen , W. C. Ren , L. B. Gao , B. L. Liu , S. F. Pei , H. M. Cheng , *Nat. Mater.* **2011**, *10*, 424.

92. X. P. Shui , D. D. L. Chung , *J. Electron. Mater.* **1997** , *26* , 928 .

93. J.Q. Ling, W.T. Zhai, W.W. Feng, B. Shen, J.F. Zhang, W.G. Zheng. *ACS Appl. Mater. & Interf.* 2013, **5(7)** 2677-2684.

94. D.X. Yan, P.G. Ren, H. Pang, Q. Fu, M.B. Yang, Z.M. Li, *J. Mater. Chem*. 2012, **22**, 18772−18774.

95. W.T. Zhai, J. Yu, L.C. Wu, W.M. Ma, J.S. He, *Polymer* 2006, **47**, 7580−7589.

96. H.C. Park, Y.P. Kim, H.Y. Kim, Y.S. Kang, *J. Membr. Sci*. 1999, **156**, 169−178.

97. W.T. Zhai, J. Wang, N. Chen, C.B. Park, H. Naguib, *Poly. Eng. Sci.* 2012, **52**,2078−2089

98. B. Krause, G.H. Koops, N.F.A.Van Der Vegt, M. Wessling, M. Wubbenhorst, *J. Adv. Mater.* 2002, **14**, 1041−1046.

99. J.C. Wang, C.S. Xiang, Q. Liu, Y.B. Pan, J.K. Guo, *Adv. Funct. Mater*. 2008, **18**, 2995−3002.

100. B. Shen, W.T. Zhai, M.M. Tao, J. Q. Ling, W.G. Zheng, *ACS Appl. Mater. & Interface* 2013, **5(21),** 11383-11391.

101. G. Sun, B. Dong, M. Cao, B. Wei, C. Hu, *Chem. Mater*. 2011, **23**, 1587−1593.

102. J. Ling, W. Zhai, W. Feng, B. Shen, J. Zhang, W. Zheng, *ACS Appl. Mater. Interfaces* 2013, **5**, 2677−2684.

103. Chae Park, H.; Po Kim, Y.; Yong Kim, H.; Soo Kang, Y. *J. Membr. Sci*. 1999, **156**, 169−

178.

104. X. Sun, J. He, G. Li, J. Tang, T. Wang, Y. Guo, H. Xue, *J. Mater. Chem*. C 2013, **1**, . 765−777.

105. P.F. Guan, X.F. Zhang, J. Guo, *Appl. Phys. Lett.* 2012, **101**, 153108.

106. R. Kumar, A. P. Singh, M. Chand, R. P. Pant, R. K. Kotnala, S. K. Dhawan, R. B. Mathur, S. R. Dhakate*, RSC Advances* 2014, **4(45),** 23476-23484.

107. T. Gupta, B.P. Singh, R.B. Mathur and S.R. Dhakate, *Nanoscale* 2014,**6**, 842-851

108. M.M. Bernal, M. Martin-Gallego, I. Molenberg, I. Huynen, M.A.L. Manchado, R. Verdejo, *RSC Adv* 2014, **4**, 7911-7918.

109. S. L. Everitt, O. G. Harlen, H. J. Wilson and D. J. Read, *J. Non Newtonian Fluid Mech.,* 2003, **114**,83–107.

110.. G. Harikrishnan, T. U. Patro, A. R. Unni and D. V. Khakhar, *Soft Matter*, 2011, **7**, 6801–6804.

111. D. Klempner and V. Sendijarevic, Handbook of polymeric foams and foam technology, Hanser Publishers, Munich, 2004.

112. R. Verdejo, R. Stamp□i, M. Alvarez-Lainez, S. Mourad, M. A. Rodriguez-Perez, P. A. Bruhwiler and M. Shaffer, *Compos. Sci. Technol*., 2009, **69**, 1564–1569.

113. O. M. Istrate and B. Chen, *Soft Matter*, 2011, **7**, 1840–1848.

114. S. T. Lee and N. S. Ramesh. Polymeric foams: mechanisms and materials, CRC Press LLC, Boca Raton, Florida, USA, 2004.

115. R. J. Pugh, *Adv. Colloid Interface Sci*., 1996, **64**,67–142.

116. F.-Q. Tang, Z. Xiao, J.-A. Tang and L. Jiang, *J. Colloid Interface Sci.,* 1989, **131**, 498–502.

117. T. Kostakis, R. Ettelaie and B. S. Murray, *Langmuir,* 2006,**22**, 1273–1280.

118. M. Martin-Gallego, M. M. Bernal, M. Hernandez, R. Verdejo and M. A. Lopez-Manchado, *Eur. Polym. J*., 2013, **49**, 1347–1353.

119. L. Chen, D. Rende, L. S. Schadler and R. Ozisik, *J. Mater. Chem. A*, 2013, **1**, 3837–3850.

120. Y. Li, X. Pei, B. Shen, W. Zhai, L. Zhang and W. Zheng, RSC Adv., 2015, 5, 24342